Lucas Formigari

Uma análise do modelo de Gutsunaev-Manko para a descrição de Rajadas Rápidas de Rádio
A analysis of the Gutsunaev-Manko model for the description of Fast Radio Bursts

São Paulo

2024

Lucas Formigari

Uma análise do modelo de Gutsunaev-Manko para a descrição de Rajadas Rápidas de Rádio
A analysis of the Gutsunaev-Manko model for the description of Fast Radio Bursts

MSc Dissertation presented at the University of São Paulo

Universidade de São Paulo

Supervisor Elcio Abdalla

São Paulo
2024

FICHA CATALOGRÁFICA
Preparada pelo Serviço de Biblioteca e Informação
do Instituto de Física da Universidade de São Paulo

Formigari, Lucas Fontana

O modelo de Gutsunaev-Manko para descrição de Rajadas Rápidas de Rádio. São Paulo, 2024.

Dissertação (Mestrado) – Universidade de São Paulo, Instituto de Física, Depto. de Física Geral.

Orientador: Prof. Dr. Élcio Abdalla

Área de Concentração: Física

Unitermos: 1. Relatividade (Física); 2. Solução de Gutsunaev-Manko; 3. Perturbações gravitacionais; 4. FRB. 5. Rajadas Rápidas de Rádio.

USP/IF/SBI-013/2024

Statement of Authorship

I hereby declare that the dissertation submitted is my own work. All direct or indirect sources used are acknowledged as references. I further declare that I have not submitted this dissertation at any other institution in order to obtain a degree.

To my friends and family. Without their help I would not have achieved anything.

Acknowledgements

This study was financed in part by the Coordenação de Aperfeiçoamento de Pessoal de Nível Superior - Brasil (CAPES) - Finance Code 001

I would like to thank my parents, for their continued support since my first days on Earth to this moment. I would also like to thank my sister for her company and encouragement.

I would like to thank my significant other, Lela Muro, for their affection and love during the production of this document. The comfort during my struggles and the company when I felt down. Their support and encouragement was vital to the production of this document.

I would also like to thank my advisor, Élcio Abdalla, for his continued support. His patience and dedication were paramount to my development as a physicist, and his guiding was foundational to the work developed here.

I would then like to thank my colleagues and professors from BINGO Collaboration. The improving and collaborative environment created by them allowed the research made here to be performed. In special, I would like to thank the professors Bertha Cuadros-Melgar, Alberto Saa, and Carlos Molina for their aid in this journey.

Finally, I would like to thank my friends who accompanied me through these years, without whom life would not be the same.

"In the beginning the Universe was created. This has made a lot of people very angry and been widely regarded as a bad move."

Douglas Adams

Abstract

In this work we discuss a magnetized solution of the Einstein Equations, that is, the Gutsunaev-Manko solution and perturbations thereof. Since Fast Radio Bursts have been suspected to be described by magnetized unstable solutions of Einstein Equations, we use that metric as a purported description of Fast Radio Bursts.

Keywords: Magnetized Axisymmetric, Fast Radio Bursts, FRB, Perturbations, Gutsanaev-Manko Solution

Resumo

Nesse trabalho é discutida uma solução magnetizada para as equações de Maxwell-Einstein, a solução de Gutsunaev-Manko e suas perturbações. Tendo em vista a suspeita de que Rajadas Rápidas de Rádio sejam descritas por soluções magnetizadas instáveis das equações de Einstein, usamos essa métrica como uma tentativa de descrever as Rajadas Rápidas de Rádio.

Palavras Chave: Magnetizados Axi-simétrico; Rajádas Rápidas de Rádio; FRB; Perturbações; Solução de Gutsunaev-Manko

List of Figures

List of Tables

Contents

1 Introduction

Several theories modifying Einstein gravity for a variety of motivations have been attempted as well as searches for cases of unstable solutions under perturbation. The latter case, concerning the search for unstable solutions, or at least unstable under certain perturbations, may have applications on physically known problems with explosive behaviour such as Fast Radio Bursts (FRB) or Gamma Ray Bursts (GRB).

Unstable solutions do exist. At least two of them have been found at both of the aforementioned cases. In the case of modifications of Einstein Gravity the stability of theories with derivative coupling is a case example widely studied in the literature (Abdalla et al., 2019a). The quasi-normal spectrum of scalar perturbations with a scalar field coupled to the Einstein tensor leads to instabilities outside the horizon of a Reissner-Nordström black hole (Chen; Jing, 2010). For higher angular momentum and derivative coupling values a region near the event horizon appears, over which the effective potential is negative valued. Thus, a phase transition may occur in a hairy black hole configuration. This effect was also investigated in (Kolyvaris et al., 2011). With the derivative coupling it was shown in (Kolyvaris et al., 2011) that there is a critical temperature below which there is a phase transition. It was also found that this hairy black hole configuration is spherically symmetric and it is thermodynamically stable having larger temperature than the corresponding Reissner-Nordström blackhole.

The quasi-normal modes (QNMs) of a test massless scalar field coupled to Einstein tensor are presented in (Minamitsuji, 2014). Additionally, various static and spherically symmetric black holes in the presence of the derivative coupling have been studied in light of their QNM in (Yu; Gao, 2019). In that scenario the oscillation frequency of QNMs became progressively smaller while their decay rate became larger as the derivative coupling was increased corroborating that the coupling of the scalar field to curvature changes the kinetic properties of the scalar field. This has also been further analysed in (Konoplya; Stuchlík; Zhidenko, 2018).

In Galileon black holes the QNMs of vectorial and spinorial perturbations were calculated again in the presence of a derivative coupling (Abdalla et al., 2019b). In this case, however, no unstable evolution was found for both spins of the perturbation. Nevertheless, Galileon black holes do present superradiant instability as was found in (Kolyvaris; Papantonopoulos, 2017; Kolyvaris et al., 2018). There, a massive charged scalar field with a coupling to the Einstein Tensor in the vicinity of the horizon of a Horndeski black hole was considered. For this scattering process the effective potential formed a negative bulge just outside the horizon, where the field can be trapped leading, in turn,

to instability. Under this scenario the conditions for superradiance were calculated as were the bound states formed in the trapping region of the potential well (Koutsoumbas; Mitsoulas; Papantonopoulos, 2018). Finally, fermionic perturbations have also been found to produce long-lived modes.

Another kind of unstable perturbation appears when variations of a Reissner-Nordstrom black hole are perturbed by a charged scalar field. As demonstrated in (Zhu et al., 2014), the response of a stable RN-dS black hole to external charged scalar perturbation is determined by the late time evolution of the perturbation. Moreover, they have shown that the late time tail of the perturbation will have a positive slope for charged scalar fields, which grows as the charge of the field is increased. As was the case in the previous examples, this instability arises from a negative valued potential well which traps the perturbative fields leading to the destabilization of the background Black Hole. Conversely, for larger charges of the perturbative field the effective potential becomes monotonic and can no longer impede the fall of the field into the horizon. In this case the late time tails become decreasing once again.

It is, thus, worthwhile studying certain perturbations of Black Hole type solutions in order to model Fast Radio Bursts. The success of the enterprise relies on having charges or other non standard couplings. In the present work magnetized solutions are considered.

This motivation comes in hand with the advance and the current construction of the BINGO radio-telescope (Abdalla et al., 2022). Named the Baryon Acoustic Oscillations from Integrated Neutral Gas Observations, it is a project comprising a collaboration between Brazil, China, France, Germany, South Africa, United Kingdom, and United States of America. It will be located in Serra da Catarina at the Municipality of Aguiar in northeast Brazil at a latitude of about 7○ south. This location was chosen in Paraiba's Outback as it combines a dry climate and a low radio interference.

As the name suggests, the main goal of the telescope is to map the Neutral Hydrogen Gas emissions, which will be done at redshifts ranging from $z = 0.127$ to $z = 0.449$, or correspondingly, at a band from 980MHz to 1260MHz. In particular, the intent is to observe so called 21cm line generated by the hyperfine structure transition. This transition is due to the split in the energy level of the ground state, based on whether the proton and the electron spins are parallel (triplet), in which the energy level is shifted up, or anti-parallel (singlet), in which it is shifted down.

This measurement allows the distribution of neutral Hydrogen atoms unbound to any molecule to be mapped. In turn, this permits matter density distribution to be studied and as such, the perturbations present in the standard model of cosmology. At the same time the frequency range means that simultaneously Radio phenomena whose emissions lie in the observation range can also be detected by the equipment including FRBs, Pulsars, among other radio transients.

This work will conduct an investigation of a candidate model for FRBs, in special, the perturbation of magnetized objects described by the Gutsunaev-Manko solution. It first begins in Chapter 2 with a brief review of some relevant description of astrophysical objects and other solutions to the Einstein equations. Then, the particular case of the Gutsunaev-Manko solution is derived, and its internal structure is studied in Chapter 3. In Chapter 4, the equations for its perturbation, together with a brief discussion on the behaviour of QNMs are considered. Finally, in Chapter 5 the numerical methods used to solve the perturbative equations are outlined and their results are presented and analyzed.

2 Einstein Equations and Astrophysical solutions

The description of gravity via Einstein Equations has a century old history. Credible, in the sense of physically relevant solutions, are on one side cosmological solutions and on the other side astrophysical solutions.

Cosmological solutions describe the Universe as a whole, its evolution, and fate. The Friedmann-Lemaître-Robertson-Walker spacetime describes a Universe filled by a Universal fluid and serves as a base for the Standard Cosmological Model. Its perturbations are a physically very relevant and presumably correct description of the Cosmos compatible with every observational fact presently known.

On the other hand, by astrophysical solutions we mean those which describe localized objects such as planets, stars, or even Black Holes. There is a plethora of such solutions, some of them quite well established such as the Schwarzschild solution and its use to approximate planet behavior around the Sun and other solutions less known, some of which are much more complex. The present work is built upon one of these, the Gutsunaev-Manko solution.

In the opposite direction, many observational phenomena in astrophysics and cosmology lack a solid theoretical understanding of their mechanisms and origins. These range from famous problems such as dark matter and dark energy to more recently discovered ones such as Fast Radio Bursts. The latter is in the core motivation for this work.

Fast Radio Bursts (FRB) are short radio transients observed in the radio frequencies, whose discovery goes back to 2007 by Lorimer et al. (Lorimer et al., 2007) from an event recorded by 64-m Parkes Telescope in 2001. As the astrophysical nature of these events were confirmed, many other detections have been made and catalogued (Petroff et al., 2016; Amiri et al., 2021). Yet the origin and mechanisms behind these events remain elusive.

They can be divided into two categories, the first containing FRB's which present a semi-periodic behaviour over extended time, while the other contains non-repeating FRB's characterized by a short duration pulse of extreme intensity. The former, however, also behave in short duration pulses and can have a quiescent period of dozens of days. As such, while the possibility of these categories representing two different phenomena cannot be discarded, non-repeating FRB might be the rarest and most energetic pulses of dimmer repeating sources (Kirsten et al., 2023; Zhang, 2020).

These pulses have a typical duration in the order of milliseconds and have been

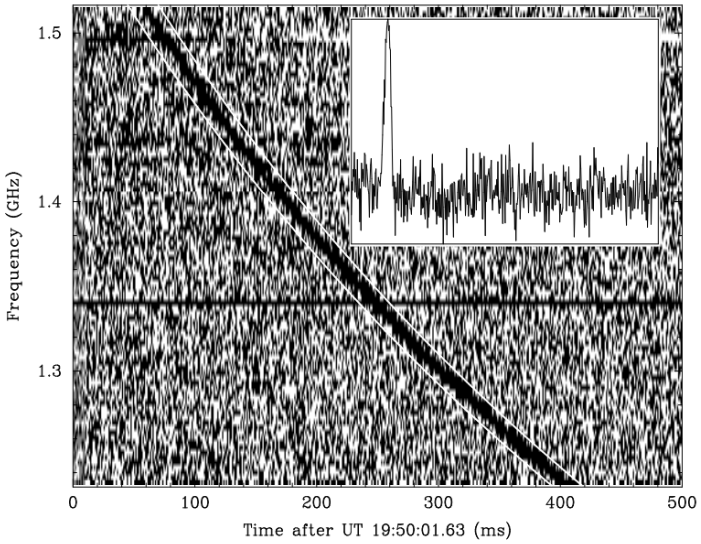

Figure 1 – The spectrogram of the first FRB observed. Image by (Lorimer et al., 2007)

observed at frequencies from $300MHz$ to $8GHz$ (Gajjar et al., 2018; Bethapudi et al., 2023). During this time their emissions reach a luminosity of up to $10^{46}erg/s$ amounting to a total emitted energy of $10^{22}g$. The pulses may have different morphology, usually with a Gaussian peak in the spectrum that chirps down as is the case with Lorimer's burst 1. However, FRB 121102 has been observed to have pulses with temporally distinct sub-bursts (Hessels et al., 2019; Li et al., 2021). The pulses are usually strongly linearly polarized, usually above 50% with FRB 121102 nearing 100% (Cordes; Chatterjee, 2019). Finally, most FRB's are located in massive galaxies with moderate to low star-formation rates consistent with a Magnetar association (Zhang, 2020).

As the emission propagates towards the Earth, it interacts with the gas and plasma from its host galaxy, from the intergalactic space, and from the Milky Way. The frequency dependent refraction index means that the lower frequency components of the burst will arrive at the detector at a later time than the higher ones explaining the chirping characteristic of the pulse. This delay called the Dispersion Measure (DM) is dependent on the free electron number density between the source and the observer and can be calculated as (Zhang, 2020)

$$\int_0^{D_z} \frac{n_e(l)}{1+z(l)} dl, \tag{2.1}$$

with D_z being the comoving distance of the source and $z(l)$ the redshift at a distance l.

Similarly, the magnetization of the propagating media causes a frequency dependent rotation of the linear polarization angle, which not only depends on the free electron number density but also on the background magnetic field parallel to the direction of propagation, $B_{||}(l)$, according to the relation,

$$\int_0^{D_z} \frac{|B_{||}(l)|^2\, n_e(l)}{(1+z(l))^2} dl. \tag{2.2}$$

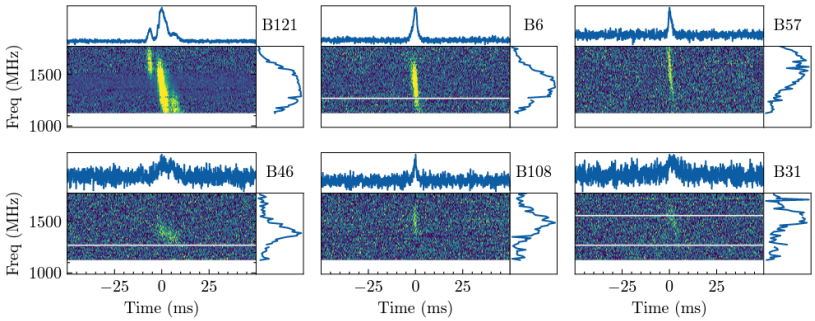

Figure 2 – The spectrogram of different observations of FRB 121102. The top left figure shows a sub-burst structure observed in this FRB. Image by (Aggarwal et al., 2021)

These two phenomena provide an extra interest in having a proper model for the emission mechanisms of FRB: an alternative source for measuring the free electron density and the magnetization of the intergalactic medium. Therefore, finding a suitable theoretical model for this phenomenon is of interest in both astrophysics and cosmology.

The models trying to describe this phenomenon must have a progenitor, i.e., an astrophysical object or collection of objects, and an emission mechanism, i.e., a physical mechanism that transfers energy from the progenitor to the electromagnetic radiation. Similarly to the observations catalogue different theoretical models have been compiled into a catalogue (Platts et al., 2019).

Candidates to progenitor generally revolve around compact objects, due to the energy budget associated to their gravitational fields, while the high linear polarization suggest a magnetized environment. However, the localization of FRB 121102 in the direction of a host galaxy whose properties are consistent with the presence of a Magnetar (Metzger; Berger; Margalit, 2017) increased the suspicion of these objects as candidates for engines.

Conversely, candidates for an emission mechanism include (Rybicki; Lightman, 1979): Bremsstrahlung Radiation, i.e., the radiation due to the deceleration of free electrons as it scatters off another electron in a plasma; Synchrotron Radiation, i.e., the radiation from the helical motion of charges along magnetic field lines; Curvature Radiation, i.e., the radiation from the acceleration of a charge due to the bending of a field line over space; and Magnetic Reconnection, i.e., the radiation from the acceleration of charges due to the relaxation of a magnetic field to a lower energy state.

In the case of the BINGO project FRB remains as one of the observational targets, together with its description in terms of a sensible model. In light of that, this work studies the magnetized solutions derived by Gutsunaev and Manko in order to find a possible engine for this kind of emission.

In order to study the GM solution, we briefly review some solutions of the general relativistic gravity as a way to provide a comparison to the target metric. In special,

Black Holes, Stars, and exploding stars are relevant to modeling FRB given the proposed location for this phenomenon.

Black holes solutions are a class of Vacuum or electrovacuum solutions of the Einstein(-Maxwell) equations, i.e., when matter fields are supposed to be zero. These objects are characterized by the existence of a horizon (Wald, 1984), a surface dividing the spacetime manifold into causally disconnected regions, i.e., no null or time-like geodesics from the interior region can cross the horizon to the exterior, although the opposite is allowed.

The first of its kind to be discovered was the Schwarzschild solution in 1916 (Schwarzschild, 2003; Schwarzschild, 1999) still in the beginnings of General Relativity. This was a static and spherically symmetric solution for a point-like mass, although its internal structure was only later understood. This solution was also fundamental in some of the early tests of Einsteinian General Relativity such as the precession of Mercury's Orbit and the gravitational lensing of light.

Not long after Schwarzschild's discovery, a similar solution for a charged object was found by Reissner (Reissner, 1916), Nordström (Nordström, 1918), Weyl (Weyl, 1917), and Jeffery (Jeffery, 1921) in 1916. This metric, called a Reissner-Nordström metric, was also a static spherically symmetric solution, which presents two distinct but concentric horizons that collapse to a single one in the limit of a vanishing charge. In fact, the metric degenerates back to the Schwarzschild one if the charge is set to zero.

The next type of black hole solution to be discovered was the Kerr metric (Kerr, 1963) in 1963. This solution represents a rotating black hole and as such is not static anymore but rather stationary as the rotation of the body causes the space to be dragged along. Furthermore, this metric is axisymmetric having an explicit dependence in the polar angle. This object also contains two horizons as in the Reissner-Nordström and also an ergosphere: a region in which an object cannot appear stationary to an outside observer. Finally, in the limit of zero angular momentum the metric once again reduces to the Schwarzschild solution.

Two years after Kerr's solution, the metric for a charged rotating black hole was found (Newman et al., 1965; Newman; Janis, 1965). This metric extends the previously discussed solutions and limits to Reissner-Nordström if the angular momentum is set to zero, to Kerr if the charge is set to zero, or finally, to Schwarzschild if both are simultaneously set to zero. The line element of this metric in Boyler-Lindquist coordinates is given by (Griffiths; Podolský, 2009),

$$ds^2 = -\frac{\Delta_r}{\rho^2}\left(dt - a\sin^2\theta d\varphi\right)^2 + \frac{\rho^2}{\Delta_r}dr^2 + \rho^2 d\theta^2 + \frac{\sin^2\theta}{\rho^2}\left(adt - (r^2+a^2)d\varphi\right)^2, \quad (2.3)$$

in which

$$\rho^2 = r^2 + a^2\cos^2\theta, \qquad \Delta_r = r^2 - 2mr + (a^2 + Q^2), \tag{2.4}$$

with a being the black hole's angular momentum divided by its mass, m being its mass and Q its charge. The horizons of this metric are found in the roots of the quadratic polynomial Δ_r,

$$r_\pm = \frac{1}{2}\left(2m \pm 2\sqrt{m^2 - a^2 - Q^2}\right). \tag{2.5}$$

Here the conditions for regularity of the Kerr-Newman solution become evident as $m^2 > a^2 + Q^2$. Additionally, the accompanying electromagnetic field is,

$$A^\mu = -\frac{Qr}{r^2 + a^2\cos^2\theta}\left[1, 0, 0, -a\sin^2\theta\right]. \tag{2.6}$$

The limiting behavior of the metric and the electromagnetic potential as r goes towards infinity is,

$$g_{tt} = -\frac{r^2 - 2mr + (a^2 + Q^2)}{r^2 + a^2\cos^2\theta} \approx -1 + \frac{2m}{r} + O(1/r^2); \tag{2.7}$$

$$A^\mu = -\frac{Q}{r}\left[1, 0, 0, -a\sin^2\theta\right], \tag{2.8}$$

which shows that the field tends to Newtonian gravitational potential for a point mass distribution, $g_{tt} = -1 + \Phi_{\text{Newton}}$. This property is called the asymptotic flatness and is expected for a solution of Einsteins-Maxwell's equations with vanishing cosmological constant.

However, the No-Hair theorem impedes further solutions to a regular asymptotically flat static Black Hole (Heusler, 1998; Bekenstein, 1998). This means that any metric that differs from Kerr-Newmann will have singularities on the outside of its horizon and, thus, cannot represent a black hole. Moreover, black holes in Einstein's gravitation are parametrized by only three parameters: their mass, angular momentum, and charge.

This limitation has sparked the interest of finding alternative models for Einstein's gravity such as coupling an scalar Dilaton field to the curvature or considering black holes in the vicinity of matter fields. In fact, the effects of Yang-Mills vector bosons (Ridgway; Weinberg, 1995; Kleihaus; Kunz, 1997), the Higgs field (Greene; Mathur; O'Neill, 1993a; Greene; Mathur; O'Neill, 1993b), and Dilaton fields (Lavrelashvili; Maison, 1993) were shown to lead to hairy black holes, i.e., black holes which differ from the Kerr-Newmann, some of them might not even present axial symmetry.

Black hole solutions mostly described vacuum or electrovacuum solutions, however, a complete description of an astrophysical object such as stars would require the consideration of the matter content in its interior. In this scenario the exterior of a non-radiating star

will still be described by a vacuum solution, while inside of a bounded region, the energy-momentum tensor will not be null but rather the one from the Lagrangian description of some other field. In fact, that was one of initial goals in Schwarzschild paper with the corresponding model being the Schwarzschild interior solution (Schwarzschild, 1999). On the surface of the star the metric and its first derivatives are usually required to be continuous even though there have been descriptions of metrics in terms of distributions (Taub, 1979).

For the description of the matter inside a simple model is to describe it in terms of a perfect fluid, i.e., an unviscous fluid which has no shear stress nor conducts any heat (Zel'dovich; Novikov; Silk, 1972). Such a fluid can be described by an energy-momentum tensor of the form,

$$T_{\mu\nu} = pg_{\mu\nu} + (\rho + p)u_\mu u_\nu, \tag{2.9}$$

with p being the pressure, ρ being the energy density, and u_μ being the 4-velocity field of the fluid. These two parameters are then related by a so called barotropic equation of state, satisfying $\rho \geq p \geq 0$ (Griffiths; Podolský, 2009). As an example, if the pressure is a linear function of the density,

$$p = (\gamma - 1)\rho, \tag{2.10}$$

with $1 \leq \gamma \leq 2$. In the limit $\gamma = 1$ the pressure of the fluid is identically zero and such a material is denominated Dust. On the other hand, using the fact that the speed of sound in the fluid is $\partial p/\partial\rho$ the limit $\gamma = 2$ corresponds to a fluid in which the speed of sound is equal to the speed of light. The latter scenario is called a stiff fluid.

Two important star solutions are: The Schwarzschild interior solution and the Tolman-Oppenheimer-Volkov (TOV) solution (Oppenheimer; Volkoff, 1939; Tolman, 1939). Both consider static spherically symmetric solutions but the former considers a constant density in the interior, while the latter takes $g_{rr} = (1 - 2\mu(r)/r)^{-1}$ with $\mu(r) = \int_0^r 4\pi r^2\rho(r)$ being the encompassed mass at a radius r. For other models one chooses different equations of state or assumes different Ansätze for the line component including relaxing some of the symmetries (Delgaty; Lake, 1998; Stephani et al., 2003).

Up to this point, the solutions discussed have been static or stationary like stars at equilibrium or black holes. However, a supernovae explosion of a star at the end of its life presents a scenario in which a star-sized expanding shell of material is radiating away during the course of up to hundreds of days (Colgate; White, 1966), to which a non-static modelling might be better suited. Conversely, Vaidya described in 1951 a metric for a

radiating star (Vaidya, 1951) compatible with a Schwarzschild solution at the beginning and the end of the radiative process. This solution, in turn, provided a framework to study supernovae in light of general relativity (Adams; Cary; Cohen, 1989).

Beyond these phenomena solutions to Einstein's equations have been derived in a variety of other contexts (**??**Stephani et al., 2003). These include cosmological solutions such as the Friedmann-Lemaître-Robertson-Walker (FLRW) describing an evolving isotropic universe and Gravitational Waves describing oscillations of the metric itself as they propagate through space (Maggiore, 2008; Maggiore, 2018). Additionally, the solutions for compact objects can be altered to describe a universe with a cosmological constant leading to asymptotically de Sitter and anti-de Sitter solutions.

3 Magnetized Axisymmetric Spacetimes

The full Einstein Equations are a set of non-linear second order tensorial partial differential equations describing the curvature of spacetime as generated by other lower spin fields (E.g. Matter Fields, the Electromagnetic field), which are coupled to their respective equations describing their dynamics such as the Klein-Gordon equation for a scalar field. In the Lagrangian formalism they can be described by the action,

$$S = \int_{\mathcal{M}} d^4x\, \mathcal{L}(g^{\mu\nu}, \partial_\lambda g^{\mu\nu}, x^\mu) = \frac{1}{16\pi} \int_{\mathcal{M}} d^4x\, \sqrt{-g}\, (R - 2\Lambda + \mathcal{L}_{ferm} + \mathcal{L}_{bos}), \tag{3.1}$$

in which R is the Ricci Scalar curvature, Λ is the Cosmological constant, $g^{\mu\nu}$ is the metric tensor, and $\mathcal{L}_{ferm}$ and $\mathcal{L}_{bos}$ are the fermionic and bosonic fields contributions, respectively. The Einstein equations can then be obtained by extremizing this integral.

For the vacuum case, i.e., when there are no other fields and so the Energy-Momentum tensor is identically null, the Ricci scalar contains terms of fourth power in the metric components and their derivatives. The effect is that finding general analytic solutions for these equations is intractable and, thus, one is led to reduce the complexity by making simplifying assumptions.

Introducing a symmetry to the spacetime has a twofold consequence. First, it reduces the number of degrees of freedom meaning a decrease in the number of variables on which the functions described by the metric and the matter fields depend, thus, reducing also the number of non-null derivatives in the equations to be solved. The second consequence is that some of the components of the metric tensor and the vector fields can be set to zero by choosing an appropriate frame of reference, thus, reducing further the number of coupled equations in the system.

One possible approach is to impose spherical symmetry as it approximates bodies that have collapsed by their own gravitational attraction from conventional stars to Black Holes. In fact, an asymptotically Euclidean static spacetime containing a perfect fluid inside a finite region with certain restrictions to the gravitational potential and to the equation of state leads to solutions with spherical symmetry (Avez, 1964; Künzle, 1971). The imposition of such symmetry to static has led to the Schwarzschild metric as well as stars solutions derived from the Tolman-Oppenheimer-Volkoff (TOV) equations for appropriate fluid descriptions (Misner; Thorne; Wheeler, 1973).

However, this type of metric is restricts the type astrophysical objects which can be modelled. The presence of a magnetic dipole, for example, imposes a preferential direction, thus, breaking the spherical symmetry. Therefore, when modeling magnetized bodies, a less restrictive imposition becomes necessary. Specifically, this dissertation will focus on

axisymmetric spacetimes.

So far, only spatial symmetries were addressed. By requiring that the spacetime possesses a one parameter group of isometries such that its orbits form time-like curves, this spacetime is called stationary (Wald, 1984). This requirement implicates a natural choice for a time coordinate, t, as the parameter of this group and the spacetime is invariant to translations in this coordinate. A further imposition is that the manifold can be foliated into space-like hypersurfaces orthogonal to the orbits of this coordinate and a spacetime fulfilling this more strict condition is called a static spacetime.

Static spacetimes allow a decomposition of the complete manifold, $\mathcal{V}_4$, into its spatial and temporal component, $\mathcal{V}_3 \times \mathbb{R}$. However, it is limited in requiring that the described object possesses no rotation neither a simultaneous electric and magnetic field. While the latter is a more reasonable assumption as charge accumulation is a infrequent phenomenon, large electric monopole fields are not reasonably expected, the former is a more imposing demand as Neutron Stars can have total angular momentum. However, as shown in (Miller; Miller; Reynolds, 2011), the values of the dimensionless angular momentum of Neutron Stars are still of the order of $a \approx 10^{-2}$, as is also the quadrupole mass moment of static stars (Laarakkers; Poisson, 1998). As such, the increase in complexity caused by the relaxation of imposing a static spacetime, both on the structure of vacuum solutions with arbitrary rotation and magnetic dipole fields as well as in the procedures to perturb such metrics, has led to the choice of limiting the scope of this thesis to keeping that stricter symmetry. In any case, a metric presenting independent magnetic and electric field is described in (Manko; Mielke; Sanabria-Gómez, 2000).

3.1 The Weyl Metric

A first step in finding a solution to the Einstein-Maxwell equations is to find an appropriate gauge. Starting from the most general metric one has for the line element

$$ds^2 = g_{\alpha\beta}\, dx^\alpha\, dx^\beta. \tag{3.2}$$

To impose the desired symmetries, the coordinates are identified as,

$$\begin{aligned} x^0 &= t; \qquad x^1 = \rho; \\ x^2 &= z; \qquad x^3 = \varphi, \end{aligned} \tag{3.3}$$

with α going from 0 to 3. Two Killing Vectors will be imposed in order to achieve stationarity and axisymmetry,

$$\xi^\alpha = (1, 0, 0, 0); \qquad \eta^\alpha = (0, 0, 0, 1). \tag{3.4}$$

Equivalently, they can be written in covariant form as,

$$\xi_\alpha = g_{\alpha\beta}\xi^\beta = g_{\alpha 0}; \qquad \eta^\alpha = g_{\alpha\beta}\eta^\beta = g_{\alpha 3}. \tag{3.5}$$

Now, requiring that the Lie derivative of the metric for the Killing vector vanishes, it leads to the Killing Equation,

$$\begin{aligned} &\mathcal{L}_\xi g = \nabla_\alpha \xi_\beta + \nabla_\beta \xi_\alpha = 0 \\ \therefore \quad &\partial_\alpha \xi_\beta + \partial_\beta \xi_\alpha - 2\Gamma^\lambda_{\alpha\beta}\xi_\lambda = \\ &\partial_\alpha g_{\beta 0} + \partial_\beta g_{\alpha 0} - 2\Gamma^\lambda_{\alpha\beta} g_{0\lambda} = 0. \end{aligned} \tag{3.6}$$

Similarly, using η_α,

$$\partial_\alpha g_{\beta 3} + \partial_\beta g_{\alpha 3} - 2\Gamma^\lambda_{\alpha\beta} g_{3\lambda} = 0. \tag{3.7}$$

Expanding the Christoffel Symbol, one arrives at

$$\begin{aligned} &\partial_\alpha g_{\beta 0} + \partial_\beta g_{\alpha 0} - 2\frac{1}{2} g^{\rho\lambda} g_{0\lambda}(\partial_\alpha g_{\beta\rho} + \partial_\beta g_{\alpha\rho} - \partial_\rho g_{\alpha\beta}) = 0 \\ &\therefore \partial_\alpha g_{\beta 0} + \partial_\beta g_{\alpha 0} - (\partial_\alpha g_{\beta 0} + \partial_\beta g_{\alpha 0} - \partial_0 g_{\alpha\beta}) = \\ &\partial_0 g_{\alpha\beta} = 0. \end{aligned} \tag{3.8}$$

Similarly, by the same imposition the derivative of the metric in relation to the coordinate φ is identically zero implying that $g_{\alpha\beta}$ is only a function of ρ and z.

Next, with the requirement of static axisymmetric spacetimes there is a space-like 2-surface orthogonal to the Killing vectors at each point of ϕ and t imposing that the induced metric only has components on the remaining coordinates, ρ and z. It can be shown that the induced metric on the surface is (Poisson, 2004),

$$h_{ab} = g_{\alpha\beta}\, e^\alpha_a e^\beta_b, \tag{3.9}$$

in which e^α_a is the tangent vector to the 2-surface. However, as the surface is spacelike and ξ and η are orthogonal to these tangent vectors, $e^0_a = e^3_a = 0$. By using the completeness relation,

$$ds^2 = \xi^\alpha \xi_\alpha dt^2 + \xi^\alpha \eta_\alpha dt d\varphi^2 + \eta^\alpha \eta_\alpha d\varphi^2 + h_{ab}\Big[e^a_\rho e^b_\rho d\rho^2 + (e^a_\rho e^b_z + e^b_\rho e^a_z) d\rho dz + e^a_z e^b_z dz^2\Big]. \tag{3.10}$$

Finally, staticity imposes there to be a hypersurface orthogonal to ξ for every value of t. Thus, from a similar argument the cross term g^{03} must also be null.

One is then left with a line element given as,

$$ds^2 = g_{00}dt^2 + g_{33}d\varphi^2 + g_{11}d\rho^2 + 2g_{12}d\rho dz + g_{22}dz^2. \tag{3.11}$$

The part of the metric comprehending ρ and z can be diagonalized by a suitable transformation of variables (Chandrasekhar, 1984). By a second transformation on the new variables

as $dz' = g_{22}/g_{11}dz$ and further on omitting the primes for the transformed coordinates, one obtains the Weyl gauge as,

$$ds^2 = -e^{2\nu}dt^2 + e^{2\psi}d\varphi^2 + e^{2\mu}(d\rho^2 + dz^2). \tag{3.12}$$

As for the Electromagnetic field potential, A_α, the Lie derivative implies,

$$\begin{aligned} \mathcal{L}_\xi A_\beta &= \xi^\alpha \partial_\alpha A_\beta + A_\alpha \partial_\beta \xi^\alpha \\ \therefore \quad \partial_0 A_\beta &= 0, \end{aligned} \tag{3.13}$$

and similarly applying it for η the derivative of the potential in the polar coordinate is also zero, thus, the electromagnetic field is only a function of ρ and z.

3.2 The Gutsunaev-Manko Solution

The Gutsunaev-Manko Solution is part of a series of solutions obtained by Manko and Sibtagulin, among others, describing the exterior field of axisymmetric objects and further on collections of objects (Manko, 1989; Manko; Sibgatullin, 1992a; Manko; Sibgatullin, 1992b; Manko, 1993). In particular, the Gutsunaev-Manko solution describes a static mass containing a Dipole Magnetic Field (Gutsunaev; Manko, 1987). Importantly, these solutions simplify to the Schwarzschild solution in the limit of a vanishing magnetic field, which leads to its interpretation as a generalization of that metric. Yet, due to the No-Hair Theorem, this modification leads to the presence of naked singularities. Thus, a physical interpretation as a Black Hole solution is not possible. Instead, it is used to represent the outside of a compact object, such as a Neutron Star, whose size is large enough to encompass all the would-be singularities.

3.2.1 Derivation of the Solution

For a Dipole Magnetic Field the potential can be given in terms of the φ component only,

$$A_\mu = \{0, 0, 0, A_\varphi(\rho, z)\}\ . \tag{3.14}$$

The Electromagnetic field is

$$\begin{aligned} B_\rho &= -\partial_z A_\varphi; \\ B_z &= \partial_\rho A_\varphi. \end{aligned} \tag{3.15}$$

For convenience, the metric is written as(Ernst, 1968a; Ernst, 1968b),

$$ds^2 = -f dt^2 + f^{-1}\left[e^{2\gamma}(d\rho^2 + dz^2) + \rho^2 d\varphi^2\right]\ . \tag{3.16}$$

In the previous equation we renamed the metric functions and re-scaled the polar coordinate as

$$\frac{d\varphi'}{d\varphi} = \frac{e^{\psi}\sqrt{f}}{\rho}. \tag{3.17}$$

Thus, the components of the Einstein tensor become,

$$G_{tt} = -\frac{e^{-2\gamma}}{4\rho}\Big\{5\rho[(\partial_\rho f)^2 + (\partial_z f)^2] - 4f(\rho\,\partial_\rho^2 f + \partial_\rho f + \rho\,\partial_z^2 f) + 4\rho f^2(\partial_\rho^2 f + \partial_z^2 f)\Big\}; \tag{3.18a}$$

$$G_{\rho\rho} = \frac{f^{-2}}{4}\Big[(\partial_\rho f)^2 - (\partial_z f)^2\Big] + \frac{\partial_\rho \gamma}{\rho}; \tag{3.18b}$$

$$G_{\rho z} = G_{z\rho} = \frac{\partial_z \gamma}{\rho} - \frac{(\partial_z f)(\partial_\rho f)}{2f^2}; \tag{3.18c}$$

$$G_{zz} = -\frac{f^{-2}}{4}\Big[(\partial_\rho f)^2 - (\partial_z f)^2\Big] - \frac{\partial_\rho \gamma}{\rho} = -G_{\rho\rho}; \tag{3.18d}$$

$$G_{\varphi\varphi} = \frac{e^{-2\gamma} f^{-2}\rho^2}{4}\Big\{[(\partial_\rho f)^2 + (\partial_z f)^2] + 4f^2(\partial_\rho^2 \gamma + \partial_z^2 \gamma)\Big\}. \tag{3.18e}$$

Meanwhile, the electromagnetic Stress-Energy tensor is given by,

$$T_{tt} = \frac{e^{-2\gamma} f^3}{2\rho^2}\Big[(\partial_\rho A_\varphi)^2 + (\partial_z A_\varphi)^2\Big]; \tag{3.19a}$$

$$T_{\rho\rho} = -T_{zz} = \frac{f}{2\rho^2}\Big[(\partial_\rho A_\varphi)^2 - (\partial_z A_\varphi)^2\Big]; \tag{3.19b}$$

$$T_{z\rho} = T_{\rho z} = \frac{f}{\rho^2}(\partial_\rho A_\varphi)(\partial_z A_\varphi); \tag{3.19c}$$

$$T_{\varphi\varphi} = \frac{e^{-2\gamma} f}{2}\Big[(\partial_\rho A_\varphi)^2 + (\partial_z A_\varphi)^2\Big]. \tag{3.19d}$$

By isolating γ and its derivative in equations for $G_{\rho\rho}$, $G_{\rho z}$, and $G_{\varphi\varphi}$, and subtracting the equation for G_{tt} from the equation for $G_{\varphi\varphi}$ multiplied by f^2/ρ^2,

$$\partial_\rho \gamma = \frac{\rho}{4}\frac{(\partial_\rho f)^2 - (\partial_z f)^2}{f^2} + \frac{f}{\rho}\left[(\partial_\rho A_\varphi)^2 - (\partial_z A_\varphi)^2\right]; \tag{3.20a}$$

$$\partial_z \gamma = \frac{\rho}{2}\frac{(\partial_\rho f)(\partial_z f)}{f^2} + \frac{2f}{\rho}\left[(\partial_\rho A_\varphi)(\partial_z A_\varphi)\right]; \tag{3.20b}$$

$$\partial_\rho^2 \gamma + \partial_z^2 \gamma = -\frac{1}{4}\frac{(\partial_\rho f)^2 + (\partial_z f)^2}{f^2} + \frac{f}{\rho^2}\left[(\partial_\rho A_\varphi)^2 + (\partial_z A_\varphi)^2\right]; \tag{3.20c}$$

$$0 = \frac{\partial_\rho^2 f + \partial_z^2 f}{f} - \frac{(\partial_\rho f)^2 + (\partial_z f)^2}{f^2} + \frac{\partial_\rho f}{\rho f} - \frac{2f}{\rho^2}\left[(\partial_\rho A_\varphi)^2 + (\partial_z A_\varphi)^2\right]. \tag{3.20d}$$

From the integrability condition of equations (3.20a) and (3.20b) and upon substituting in equation (3.20c), with the help of equation (3.20d), one arrives at (Gutsunaev; Manko, 1988; Freitas, 2013; Filho, 2020):

$$\vec{\nabla}\left(\frac{f}{\rho^2}\vec{\nabla}A_\varphi\right) = 0; \tag{3.21a}$$

$$\vec{\nabla}\left(\frac{1}{f}\vec{\nabla}f - \frac{2f}{\rho^2}A_\varphi\vec{\nabla}A_\varphi\right) = 0; \tag{3.21b}$$

in which the operator

$$\vec{\nabla} = \hat{\rho}\partial_\rho + \hat{z}\partial_z \tag{3.22}$$

was introduced.

It is also convenient to introduce a change of variables to prolate spheroidal coordinates. For such a coordinate system two foci are chosen along the z-axis, equidistant to the origin by a parameter k. This leads to the transformations,

$$\begin{cases} x = \sqrt{\rho^2 + (z+k)^2} + \sqrt{\rho^2 + (z-k)^2}\,; \\ y = \sqrt{\rho^2 + (z+k)^2} - \sqrt{\rho^2 + (z-k)^2}\,; \end{cases} . \tag{3.23}$$

Likewise, the inverse transformation is,

$$\begin{cases} \rho = k\sqrt{(x^2-1)(1-y^2)}\,; \\ z = kxy \quad . \end{cases} \tag{3.24}$$

The operator $\vec{\nabla}$ turns into

$$\vec{\nabla} = \frac{1}{k\sqrt{x^2-y^2}}\left(\hat{x}\sqrt{x^2-1}\partial_x + \hat{y}\sqrt{1-y^2}\partial_y\right), \tag{3.25}$$

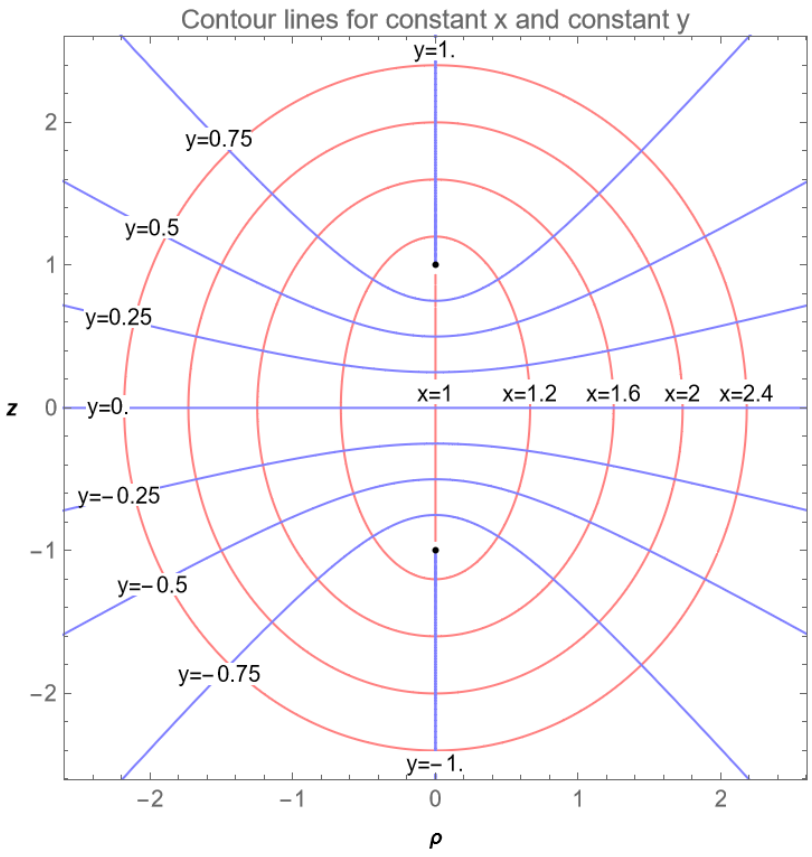

Figure 3 – Contour lines for constant x and constant y on the plane ρz with k=1

while its square becomes

$$\nabla^2 = \frac{1}{k^2(x^2-y^2)}\left\{\partial_x[(x^2-1)\partial_x] + \partial_y[(1-y^2)\partial_y]\right\} \quad . \tag{3.26}$$

With this parametrization lines of constant x are ellipses whose foci are in $z = \pm k$, while lines of constant y are hyperbolae whose foci also lie in these two points. X is defined in the interval $[1, \infty) \subset \mathbb{R}$ degenerating into the line from -1 to 1 on the z-axis, whereas Y is defined in the interval $[-1, 1] \subset \mathbb{R}$ and degenerates to the line segments on the z-axis comprising $z > 1$ and $z < -1$ for $y \to 1$ and $y \to -1$, respectively. This can be seen in figure 3. Additionally, the $z = 0$ plane is covered by $y = 0$.

The equations (3.21a) and (3.21b) thus become,

$$\partial_x\left(\frac{f}{1-y^2}\partial_x A_\varphi\right) + \partial_y\left(\frac{f}{x^2-1}\partial_y A_\varphi\right) = 0; \tag{3.27a}$$

$$\partial_x\left(\frac{(x^2-1)}{f}\partial_x f - \frac{2A_\varphi f}{k^2(1-y^2)}\partial_x A_\phi\right) + \partial_y\left(\frac{(1-y^2)}{f}\partial_y f - \frac{2A_\phi f}{k^2(x^2-1)}\partial_y A_\varphi\right) = 0 \quad . \tag{3.27b}$$

In order to arrive at Ernst equations, we define to new variables as (Gutsunaev; Manko, 1988),

$$\epsilon_1 = \sqrt{f} + A'_\varphi; \qquad \epsilon_2 = \sqrt{f} - A'_\varphi; \tag{3.28}$$

with the potential A'_φ defined to automatically satisfy (Ernst, 1968b),

$$\hat{\varphi} \times \vec{\nabla} A'_\varphi = \frac{f}{\rho} \vec{\nabla} A_\varphi, \tag{3.29}$$

or in the coordinate form,

$$\partial_x A'_\varphi = \frac{f\, \partial_y A_\varphi}{k(x^2-1)}; \quad \partial_y A'_\varphi = -\frac{f\, \partial_x A_\varphi}{k(1-y^2)}. \tag{3.30}$$

By substituting the potentials defined in equation (3.28) into equations (3.27a) and (3.27b), the Ernst equations are obtained,

$$(\epsilon_1 + \epsilon_2)\vec{\nabla}^2 \epsilon_1 = 2(\vec{\nabla}\epsilon_1)^2; \tag{3.31a}$$

$$(\epsilon_1 + \epsilon_2)\vec{\nabla}^2 \epsilon_2 = 2(\vec{\nabla}\epsilon_2)^2. \tag{3.31b}$$

As given in (Gutsunaev; Manko, 1988), if two functions ϵ_1^0 and ϵ_2^0 are solutions to the Ernst Equations, so are

$$\epsilon_1 = \epsilon_1^0 - \frac{(\epsilon_1^0 + \epsilon_2^0)(1-A)(1-B)}{x(1-AB) + y(B-A) + (1-A)(1-B)}; \tag{3.32a}$$

$$\epsilon_2 = \epsilon_2^0 - \frac{(\epsilon_1^0 + \epsilon_2^0)(1+A)(1+B)}{x(1-AB) - y(B-A) + (1+A)(1+B)}; \tag{3.32b}$$

defined such that A and B satisfy the equations,

$$\begin{aligned} &2(x-y)(\epsilon_1^0 + \epsilon_2^0)\, \partial_x A \\ &\quad = 2A\hat{N}_1^{(-)}(\epsilon_1^0 + \epsilon_2^0) + \left[(1+A^2)\hat{N}_1^{(-)} - (x-y)(1-A^2)\partial_x\right](\epsilon_1^0 - \epsilon_2^0); \end{aligned} \tag{3.33a}$$

$$\begin{aligned} &2(x-y)(\epsilon_1^0 + \epsilon_2^0)\, \partial_y A \\ &\quad = 2A\hat{N}_2^{(-)}(\epsilon_1^0 + \epsilon_2^0) + \left[(1+A^2)\hat{N}_2^{(-)} - (x-y)(1-A^2)\partial_y\right](\epsilon_1^0 - \epsilon_2^0); \end{aligned} \tag{3.33b}$$

$$\begin{aligned} &-2(x+y)(\epsilon_1^0 + \epsilon_2^0)\, \partial_x B \\ &\quad = 2A\hat{N}_1^{(+)}(\epsilon_1^0 + \epsilon_2^0) + \left[(1+B^2)\hat{N}_1^{(+)} + (x+y)(1-B^2)\partial_x\right](\epsilon_1^0 - \epsilon_2^0); \end{aligned} \tag{3.33c}$$

$$\begin{aligned} &-2(x+y)(\epsilon_1^0 + \epsilon_2^0)\, \partial_y B \\ &\quad = 2A\hat{N}_2^{(+)}(\epsilon_1^0 + \epsilon_2^0) + \left[(1+B^2)\hat{N}_2^{(+)} + (x+y)(1-B^2)\partial_y\right](\epsilon_1^0 - \epsilon_2^0). \end{aligned} \tag{3.33d}$$

In this set of equations the operators $N_1^{(\pm)}$ and $N_2^{(\pm)}$ are defined as (Gutsunaev; Manko, 1988),

$$\hat{N}_1^{(\pm)} \equiv (xy \pm 1)\partial_x + (1-y^2)\partial_y; \qquad \hat{N}_2^{(\pm)} \equiv -(x^2-1)\partial_x + (xy \pm 1)\partial_y. \tag{3.34}$$

Now, setting $A_3' = 0$ leads to $\epsilon_1^0 = \epsilon_2^0 = \sqrt{f} = \exp(\psi)$, such that,

$$\vec{\nabla}^2\psi = 0, \tag{3.35}$$

i.e., ψ is any solution of the 2-d Laplace equation in prolate spheroidal coordinates,

$$\psi = -\frac{1}{2}\ln\left(\frac{x-1}{x+1}\right) + \alpha_n \hat{L}_n \ln\left(\frac{x-1}{x+1}\right), \quad \text{for } n = 1, 2, \ldots \tag{3.36}$$

The selection of α_n allows the generation of solutions with mass multipole moments. For the desired solution all multipole moments should be predictable from the total mass, which has already been set to one by the initial choice of a system of unities. As a consequence, there should be only one parameter that should describe the magnetic field. Thus, just the first parameter, α_0, is kept while the others are set to zero, i.e., $\alpha_n = 0$ for all $n \geq 1$. With these impositions equations (3.33a) to (3.33d) become,

$$\partial_x A = \frac{A}{(x-y)}\left[(xy-1)\partial_x\psi + (1-y^2)\partial_y\psi\right]; \tag{3.37a}$$

$$\partial_y A = \frac{A}{(x-y)}\left[-(x^2-1)\partial_x\psi + (xy-1)\partial_y\psi\right]; \tag{3.37b}$$

$$\partial_x B = \frac{B}{(x+y)}\left[(xy+1)\partial_x\psi + (1-y^2)\partial_y\psi\right]; \tag{3.37c}$$

$$\partial_y B = \frac{B}{(x+y)}\left[-(x^2-1)\partial_x\psi + (xy+1)\partial_y\psi\right]; \tag{3.37d}$$

which admit solutions of the form,

$$A = \alpha_0\frac{\sqrt{(x^2-1)}}{(x-y)}; \qquad B = \beta_0\frac{\sqrt{(x^2-1)}}{(x+y)}. \tag{3.38}$$

In equation (3.38) α_0 and β_0 are integration constants. These are then particularized for $\alpha_0 = \beta_0$, and substituted back in equation (3.32a) and (3.32b), which allows the Ernst Potentials to be explicitly derived as,

$$\epsilon_1 = \sqrt{\frac{x-1}{x+1}}\,\frac{x^2-y^2+\alpha_0^2(x+1)^2 - 2\alpha_0 y\sqrt{x^2-1}}{x^2-y^2+\alpha_0^2(x-1)^2 - 2\alpha_0 y\sqrt{x^2-)}}; \tag{3.39a}$$

$$\epsilon_2 = \sqrt{\frac{x-1}{x+1}}\,\frac{x^2-y^2+\alpha_0^2(x+1)^2+2\alpha_0 y\sqrt{x^2-1}}{x^2-y^2+\alpha_0^2(x-1)^2+2\alpha_0 y\sqrt{x^2-1}}. \tag{3.39b}$$

Once that the potentials have been calculated, a substitution on their definition in equation (3.28) produces the metric function,

$$f = \frac{x-1}{x+1}\left\{\frac{[x^2-y^2+\alpha_0^2(x^2-1)]^2+4\alpha_0 x^2(1-y^2)}{[x^2-y^2+\alpha_0^2(x-1)^2]^2-4\alpha_0 y^2(x^2-1)}\right\}^2, \tag{3.40}$$

and the electromagnetic potential,

$$A'_\varphi = \frac{8\alpha_0^3 xy(x-1)}{[x^2-y^2+\alpha_0^2(x-1)^2]^2-4\alpha_0 y^2(x^2-1)}. \tag{3.41}$$

In turn, f and A'_φ can be used to integrate the equations (3.30), (3.20a) (3.20b), resulting in polar electromagnetic potential,

$$A_\varphi = \frac{4k\alpha_0^3(1-y^2)[2(1+\alpha_0^2)x^3+(1-3\alpha_0^3)x^2+y^2+\alpha_0^2]}{(1+\alpha_0^2)\{[x^2-y^2+\alpha_0^2(x^2-1)]^2+4\alpha_0 y^2(x^2-1)\}}, \tag{3.42}$$

and the metric function,

$$e^{2\gamma} = \frac{x^2-1}{x^2-y^2}\,\frac{\{[x^2-y^2+\alpha_0^2(x^2-1)]^2+4\alpha_0 x^2(1-y^2)\}^4}{(1+\alpha_0^2)^8(x^2-y^2)^8}. \tag{3.43}$$

As shown in (Gutsunaev; Manko, 1987), the metric functions can be transformed into a spherical form which can be compared back to the Schwarzschild solution. This is done with a choice of the prolate spheroidal scale factor, $k = m(1+\alpha^2)/(1-3\alpha^2)$, and a subsequent change of variables with $y = \cos(\theta)$ and $x = (r-m)/k$. In this new coordinate system the asymptotic behavior of f and A_3 at infinity is,

$$f = 1 - \frac{2m}{r} + O(r^{-3}), \tag{3.44}$$

and,

$$A_\varphi = 8\frac{m^2\alpha^3}{(1-3\alpha^2)^2 r}\sin^2(\theta) + O(r^{-2}). \tag{3.45}$$

By recalling that in the Weyl gauge the metric function f corresponds to the time-time component of the metric tensor, the first two terms in the RHS of equation (3.44) correspond to the weak field limit potential of a massive point distribution. Similarly, the first term of the RHS of equation (3.45) corresponds to the polar term of the electromagnetic potential of a magnetic dipole aligned with the z-axis. Thus, the mass and magnetic dipole moment of the objects described by this solution can be identified as,

$$m = k\frac{(1-3\alpha^2)}{1+\alpha^2}; \tag{3.46a}$$

$$\mu = \frac{8m^2\alpha^3}{(1-3\alpha^2)^2} = \frac{8k^2\alpha^3}{(1+\alpha^2)^2}. \tag{3.46b}$$

In the scenario of a vanishing magnetic field, i.e., $\alpha \to 0$, the metric returns to Schwarzschild by using these same transformations,

$$f = \frac{x-1}{x+1} = \frac{r-2m}{r} = \left(1 - \frac{2m}{r}\right). \tag{3.47}$$

3.2.2 Internal Structure of the Metric

In order to better study the structure and the perturbations of this metric, the metric functions can be rewritten as,

$$ds^2 = -\left(\frac{x-1}{x+1}\right) f^2 dt^2 + \left(\frac{g}{f}\right)^2 \left(\frac{x+1}{x-1}dx^2 + \frac{(x+1)^2}{1-y^2}dy^2\right) + \frac{(x+1)^2(1-y^2)}{f^2}d\phi^2, \tag{3.48}$$

in which f and g will be

$$f = \frac{(x^2-y^2+\alpha^2(x^2-1))^2 + 4\alpha^2x^2(1-y^2)}{(x^2-y^2+\alpha^2(x-1)^2)^2 - 4\alpha^2y^2(x^2-1)}, \tag{3.49}$$

and

$$g = \frac{\left((x^2-y^2+\alpha^2(x^2-1))^2 + 4\alpha^2x^2(1-y^2)\right)^2}{(\alpha^2+1)^4(x^2-y^2)^4}. \tag{3.50}$$

In this new scenario taking the Schwarzschild limit, $\alpha = 0$, makes,

$$f = 1, \qquad g = 1. \tag{3.51}$$

In this gauge it becomes apparent that the function f and the ratio between f and g serve as deformations to the Schwarzschild metric caused by the presence of the magnetic dipole. For this comparison it is useful to transform back into the coordinates $x = (r-m)/k$ and $y = \cos(\theta)$, in which the line element is explicitly

$$ds^2 = -\left(1 - \frac{2k}{r-(m-k)}\right) f^2 dt^2 + \left(\frac{g}{f}\right)^2 \left\{\left(1 - \frac{2k}{r-(m-k)}\right)^{-1} dr^2 + [r-(m-k)]^2 d\theta^2\right\} + \frac{[r-(m-k)]^2(\sin\theta^2)}{f^2}d\phi^2. \tag{3.52}$$

These coordinates reveal that the radial dependence happens in a dislocated radius by a factor of $(m-k)$, which is encapsulated by the prolate spheroidal variable x, while the dependence on the mass is modified to a dependence on the scale factor $k = m(1+\alpha^2)/(1-3\alpha^3)$.

The representation of the line element given by equation (3.48) highlights some regions of interest where a metric component either vanishes or diverges. A first such case is when $x = 1$. This corresponds to the Schwarzschild horizon as seen in the limit of $\alpha \to 0$. However, in view of this limit it is worth noting that the apparent divergence due to $y \to 1$ can be simply transformed away by choosing $y = \cos\vartheta$, as

$$g_{yy}dy^2 = \frac{(x+1)^2}{1-\cos^2\vartheta}\sin^2\vartheta d\vartheta^2 = (x+1)^2 d\vartheta^2. \tag{3.53}$$

Thus, the remaining regions of interest are the zeroes and poles of f and g/f. The numerator of the former is a sum of squared real terms and, thus, is only null if both are zero that only happens at $x = y = 1$, in which

$$\lim_{(x,y)\to(1,1)} f = 0; \qquad \lim_{(x,y)\to(1,1)} g = 1. \tag{3.54}$$

In turn, this justifies investigating the metric structure in this region as g/f also diverges.

Finally, the denominator of f can also be zero at the roots of

$$(x^2 - y^2 + \alpha^2(x-1)^2)^2 - 4\alpha^2 y^2(x^2-1) = 0, \qquad x \geq 1, y \leq 1, \tag{3.55}$$

which can admit up to four positive solutions for x. The exact form involves nested square roots of rational functions in α and y. However, the boundaries of the singular region can be found by extremizing the implicit equation (3.55). Thus, both the upper and lower limits for x are found in the polar axis, i.e. $y = \pm 1$, with the former on the points $x = \pm y = 1$. Conversely, the range of values for y range from zero to its minimal value given by,

$$y^2 = \frac{[x^3 + \alpha^2(x-1)^2]\,[x + \alpha^2(x-1)]}{[x + \alpha^2(x-1) + 2\alpha^2 x^2]}. \tag{3.56}$$

Once again, the value of x at that position can be determined by inserting y^2 back into equation (3.55). Above these values there are values of x for which the metric tensor's component g_{tt} diverges. This divergence, in turn, is an indication that there might be a spacetime singularity there, which still has to be contrasted from a coordinate singularity as was the case with the limit $y \to 1$.

The candidate singular region will be located around the poles of the black hole, just outside of the horizon as can be seen in figure 4. On one hand, the maximum angle from the z-axis is given by equation (3.56) and for a near-extreme solution, i.e., when $\alpha = 1/\sqrt{3}$, what is circa 30°. On the other had, the maximum distance from the horizon that the singularity achieves is reached at the poles and in the same near-extreme case it would have coordinate position equal to $x \approx 1.48$. Moreover, the singularity curves back and touches the horizon at both poles, i.e., $x = y = 1$. At this point, however, the function f is regular and vanishes as shown in equations (3.54).

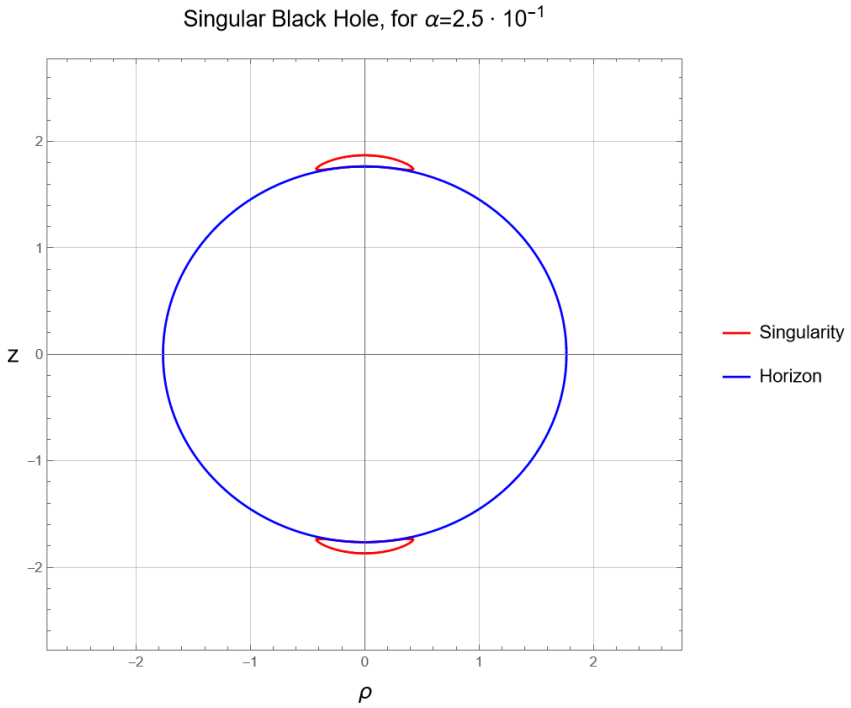

Figure 4 – Horizon and Singularities for the Gutsunnaev-Manko Metric, with $\alpha = 0.25$ and $k = 1$

To analyze the behavior of the metric near these points of interest in a coordinate independent manner, the null geodesics should be studied. Starting at the geodesics for constant φ the initial 4-velocity is normalized as,

$$u^{\alpha}_{(0)} u^{\beta}_{(0)} g_{\alpha\beta} = 0$$
$$\therefore (u^{t}_{(0)})^2 = -\frac{g_{xx}(u^{x}_{(0)})^2 + g_{yy}(u^{y}_{(0)})^2}{g_{tt}}. \tag{3.57}$$

Then, in the geodesic equation for the φ component, we check whether it is possible for a particle to radially fall into the star without acquiring a polar angular velocity. While this is always possible in Newtonian physics, this is not the case in General Relativity, as shown by the Geodesics around a Kerr black hole (Chandrasekhar, 1984). The proper-time derivative of the angular velocity is,

$$\frac{du^{\varphi}}{d\tau} = -\Gamma^{\varphi}_{\alpha\beta} u^{\alpha} u^{\beta} = -2\Gamma^{\varphi}_{x\varphi} u^{x} u^{\varphi} - 2\Gamma^{\varphi}_{y\varphi} u^{y} u^{\varphi}, \tag{3.58}$$

which means that the acceleration for this component also vanishes in the case of a null initial velocity. As equation (3.58) is a first order differential equation with both initial value and initial derivative equal to zero, the particular solution is identically zero. Therefore, the angular velocity will remain zero and, consequently, x^{φ} will remain constant.

Now, expanding the equation for the x and y components, we have

$$\frac{du^x}{d\tau} = -\Gamma^x_{tt}(u^t)^2 - \Gamma^x_{xx}(u^x)^2 - 2\,\Gamma^x_{xy}(u^y)(u^x) - \Gamma^x_{yy}(u^y)^2; \tag{3.59}$$

$$\frac{du^y}{d\tau} = -\Gamma^y_{tt}(u^t)^2 - \Gamma^y_{xx}(u^x)^2 - 2\,\Gamma^y_{xy}(u^y)(u^x) - \Gamma^y_{yy}(u^y)^2. \tag{3.60}$$

The value u^t obtained from the normalization requirement, equation (3.57), can be substituted in these two equations. Grouping similar terms, one arrives at the geodesic equations in terms only of the x and y components of the 4-velocity,

$$\frac{du^x}{d\tau} = -\left[\Gamma^x_{xx} - \Gamma^x_{tt}\frac{g_{xx}}{g_{tt}}\right](u^x)^2 - \left[\Gamma^x_{yy} - \Gamma^x_{tt}\frac{g_{yy}}{g_{tt}}\right](u^y)^2 - 2\,\Gamma^x_{xy}(u^y)(u^x)\ ; \tag{3.61}$$

$$\frac{du^y}{d\tau} = -\left[\Gamma^y_{xx} - \Gamma^y_{tt}\frac{g_{xx}}{g_{tt}}\right](u^x)^2 - \left[\Gamma^y_{yy} - \Gamma^y_{tt}\frac{g_{yy}}{g_{tt}}\right](u^y)^2 - 2\,\Gamma^y_{xy}(u^y)(u^x)\ . \tag{3.62}$$

The mixing of u^x and u^y in the above equations implies that the null geodesics will not trace a constant y or constant x curve for a generic case. Nevertheless, in the plane $y = 0$,

$$-\left[\Gamma^x_{yy} - \Gamma^x_{tt}\frac{g_{yy}}{g_{tt}}\right] = 0, \tag{3.63}$$

In this case equation (3.61) reduces to,

$$\begin{aligned}\frac{du^x}{d\tau} &= -\left[\Gamma^x_{xx} - \Gamma^x_{tt}\frac{g_{xx}}{g_{tt}}\right](u^x)^2 = -\left.\frac{\partial_x g}{g}\right|_{y=0}(u^x)^2 \\ &= \frac{8\alpha^2\left(\alpha^2 + x^2(1-\alpha^2)\right)}{x\left(\alpha^4 + x^4(1+\alpha^2) + 2x^2\alpha^2(1-\alpha^2)\right)}(u^x)^2 \quad .\end{aligned} \tag{3.64}$$

This shows that the radial component of the 4-velocity in the proper-time remains regular at $x = 1$ as is expected on an event horizon. In contrast, by expressing both equations in terms of the time derivative, the geodesic equations for x and y take the form ,

$$\frac{d^2x}{dt^2} = -\Gamma^x_{tt} + \left[2\Gamma^t_{tx} - \Gamma^x_{xx}\right]\left(\frac{dx}{dt}\right)^2 + \left[2\Gamma^t_{ty} - \Gamma^x_{xy}\right]\left(\frac{dx}{dt}\right)\left(\frac{dy}{dt}\right) - \Gamma^x_{yy}\left(\frac{dy}{dt}\right)^2\ ; \tag{3.65}$$

$$\frac{d^2y}{dt^2} = -\Gamma^y_{tt} + \left[2\Gamma^t_{ty} - \Gamma^y_{yy}\right]\left(\frac{dy}{dt}\right)^2 + \left[2\Gamma^t_{tx} - \Gamma^y_{xy}\right]\left(\frac{dx}{dt}\right)\left(\frac{dy}{dt}\right) - \Gamma^y_{xx}\left(\frac{dx}{dt}\right)^2\ . \tag{3.66}$$

If the scenario of radial infall in the equatorial plane is considered again, the 4-velocity will satisfy the null-geodesic normalization, given in equation (3.57),

$$\frac{dx}{dt} = \left(\frac{dt}{d\tau}\right)^{-1}\frac{dx}{d\tau} = \sqrt{\frac{-g_{tt}}{g_{xx}}}. \tag{3.67}$$

This value goes to zero as x approaches 1 showing that the redshift of a photon travelling along this curve would increase indefinitely as it also approaches the surface $x = 1$. Finally,

if this result is substituted in the geodesic equations,

$$\frac{d^2x}{dt^2} = -\Gamma^x_{tt} - \left[2\Gamma^t_{tx} - \Gamma^x_{xx}\right]\frac{g_{tt}}{g_{xx}} \quad ; \tag{3.68}$$

$$\frac{d^2y}{dt^2} = 0 \quad . \tag{3.69}$$

Thus, in the equatorial plane the derivative of the speed is bounded and goes to zero as the curve approaches $x = 1$. Thus, in addition to the regularity of the Ricci Scalar curvature, given in appendix A.2, this means that the surface defined by $x = 1$ is a event horizon as is the case for the Schwarzschild Metric. A similar argument can be constructed for every point by which the surface can be approached with the exception of the poles.

Conversely, approaching the surface over which f diverges, as defined by equation (**??**), the terms Γ^x_{tt} and Γ^y_{tt} diverge. This confirms the suspicion that this surface is indeed a singular region of spacetime. At the poles, in particular, these two terms are regular and vanish, but all other Christoffel Symbols in equations (3.65) and (3.66) diverge. The summarized structure of the horizon and singularities can be seen in figure 4.

4 Metric Perturbations

So far, the solution for the metric has been derived for vacuum outside a bounded region of space in a highly symmetric and stationary case. While these simplifications were fundamental in obtaining a solution to the Einstein Equations, they provide little information on how to probe such objects as there are no observable fields interacting with it; nor is there any radiative behavior. As such, there is interest in exploring how such a solution behaves in the presence of an additional structure around it.

Adding an extra field or breaking some symmetry of the original metric is not an easy task. Due to the non-linearity of Einstein-Maxwell's equations and their intricate coupling to matter fields, adding a field to a solution would mean, in the general case, having to solve the whole system again as one did to obtain the background metric in the first case. This difficulty coupled to the extreme energies involved in Compact Objects suggests perturbative methods as a viable candidate for studying such extensions of the original solution.

To arrive at the perturbative behavior of the solution (Wald, 1984), a family of solutions to the Einstein-Maxwell equations, $\left\{\tilde{g}_{\mu\nu}(\varepsilon), \tilde{A}^{\mu}(\varepsilon)\right\}$ parametrized by ε is supposed to exist. They are then expanded as a Taylor Series in terms of ε leading to,

$$\tilde{g}_{\mu\nu}(\varepsilon) = g_{\mu\nu} + \varepsilon h_{\mu\nu} + O(\varepsilon^2); \tag{4.1}$$

$$\tilde{A}^{\mu} = A^{\mu\,(0)} + \varepsilon A^{\mu\,(1)} + O(\varepsilon^2). \tag{4.2}$$

The field equations can thus be expanded as (Pound; Wardell, 2021),

$$G^{(0)}_{\mu\nu} + \varepsilon G^{(1)}_{\mu\nu} + O(\varepsilon^2) = T^{(0)}_{\mu\nu} + \varepsilon \left({}^{(grav)}T^{(1)}_{\mu\nu} + {}^{(EM)}\,T^{(1)}_{\mu\nu} + {}^{(matter)}\,T^{(1)}_{\mu\nu}\right) + O(\varepsilon^2); \tag{4.3}$$

$$\nabla_{\mu}\left(F^{\mu\nu} + \varepsilon \mathcal{F}^{\mu\nu} + O(\varepsilon^2)\right) = \varepsilon J^{\nu\,(1)} + O(\varepsilon^2). \tag{4.4}$$

This leads to the first-order perturbative equations,

$$G^{(1)}_{\mu\nu} = {}^{(grav)}\,T^{(1)}_{\mu\nu} + {}^{(EM)}\,T^{(1)}_{\mu\nu} + {}^{(matter)}\,T^{(1)}_{\mu\nu}; \tag{4.5}$$

$$\nabla_{\mu}\mathcal{F}^{\mu\nu} = J^{\nu\,(1)}; \tag{4.6}$$

in which the first order perturbation of the Einstein Tensor, $G^{(1)}_{\mu\nu}$, the electromagnetic, ${}^{(EM)}T^{(1)}_{\mu\nu}$, and gravitational, ${}^{(grav)}T^{(1)}_{\mu\nu}$, components of the Stress-Energy Tensor, and the

Electromagnetic Tensor, $\mathcal{F}^{\mu\nu}$, are given by,

$$G^{(1)}_{\mu\nu} = R^{(1)}_{\mu\nu} - \frac{1}{2}g_{\mu\nu}R^{(1)} + (h^{\alpha}{}_{\mu}g^{\beta}{}_{\nu} + g^{\alpha}{}_{\mu}h^{\beta}{}_{\nu} - \frac{1}{2}g_{\mu\nu}h^{\alpha\beta})R^{(0)}_{\alpha\beta} - \frac{1}{2}h_{\mu\nu}R^{(0)}; \tag{4.7}$$

$${}^{(grav)}T^{(1)}_{\mu\nu} = h_{\mu\alpha}F^{\alpha}{}_{\beta}F^{\beta}{}_{\nu} + h_{\nu\alpha}F^{\alpha}{}_{\beta}F^{\beta}{}_{\mu} - h_{\alpha\beta}F^{\alpha}{}_{\mu}F^{\beta}{}_{\nu} + \frac{1}{4}h_{\alpha\beta}F_{\lambda\delta}F^{\lambda\delta} + \frac{1}{2}g_{\mu\nu}h_{\alpha\beta}F^{\alpha}_{\lambda}F^{\lambda\beta}; \tag{4.8}$$

$${}^{(EM)}T^{(1)}_{\mu\nu} = -(g_{\mu\alpha}F_{\nu\lambda}\mathcal{F}^{\alpha\lambda} + g_{\nu\lambda}F_{\mu\alpha}\mathcal{F}^{\alpha\lambda} - \frac{1}{2}g_{\mu\nu}F_{\alpha\lambda}\mathcal{F}^{\alpha\lambda}); \tag{4.9}$$

$$\mathcal{F}^{\mu\nu} = h^{\mu\lambda}\nabla_{\lambda}A^{\nu\,(0)} - h^{\nu\lambda}\nabla_{\lambda}A^{\mu\,(0)} + g^{\mu\lambda}\nabla_{\lambda}A^{\nu\,(1)} - g^{\nu\lambda}\nabla_{\lambda}A^{\mu\,(1)}; \tag{4.10}$$

$$R^{(1)}_{\mu\nu} = \frac{1}{2}\left(\nabla_{\alpha}\nabla_{\mu}h^{\alpha}_{\nu} + \nabla_{\alpha}\nabla_{\nu}h^{\alpha}_{\mu} - \nabla^2 h_{\mu\nu} - \nabla_{\mu}\nabla_{\nu}h\right) \tag{4.11}$$

$$R^{(1)} = -h^{\mu\nu}R^{(0)}_{\mu\nu} + \nabla_{\mu}\nabla_{\nu}h^{\mu\nu} - \nabla^2 h \tag{4.12}$$

Additionally, the Four-Current, $J^{\nu\,(1)}$, and the matter component of the Stress-Energy Tensor, ${}^{(matter)}T^{(1)}_{\mu\nu}$, are caused by the introduction of perturbative matter fields and will vanish for purely electromagnetic and gravitational perturbations.

As seen in equations (4.7) to (4.12) a coupling between the gravitational and the electromagnetic first-order equations arises so that an initially purely gravitational mode (conversely, purely electromagnetic) excites electromagnetic (gravitational) modes. In fact, even an uncharged matter field can induce electromagnetic waves through the production of gravitational waves as it travels around a magnetized compact object. In this scenario, the matter field would serve as a source in equation (4.5), although equation (4.6) remains homogeneous.

This interconnection implies a higher difficulty in generating solutions to these equations. The metric no longer has the symmetries that allowed for a separation of variables as is possible for the Schwarzschild or Reissner-Nordström cases, in which a hyperbolic equation for a single variable could be studied. However, if the evolution of matter fields in the periphery of such an object is found to be unstable, this would also imply a runoff of electromagnetic and gravitational radiation leading to a description of an explosive event.

4.1 Classification of Perturbations by Spin

The perturbative metric and electromagnetic potential described in equations (4.1) and (4.2) were written in their full generality. As a consequence, it does not take into account the symmetries provided by the background metrics, which can provide a simplification for the perturbation equations (4.7) to (4.9). In spherically symmetric metrics, for example, the equations should stay invariant by rotations and as such, the angular variables, θ and φ, should be separable from the radial and time variables, r and t.

It is worth then to look at how the metric transforms under rotation by an angle $\hat{\phi}$ around an axis $\hat{\mathbf{n}}$ in spherical coordinates,

$$h'_{\mu\nu} = \frac{dx^\alpha}{dx'^\mu}\frac{dx^\beta}{dx'^\nu}h_{\alpha\beta}; \tag{4.13}$$

$$\frac{dx^\alpha}{dx'^\mu} = \left[\delta^\alpha_{t'}\delta^t_\mu + \delta^\alpha_{r'}\delta^r_\mu + R^\alpha_\mu(\hat{\mathbf{n}},\hat{\phi})\right]; \tag{4.14}$$

with $R^\alpha_\mu(\hat{\mathbf{n}},\hat{\phi})$ being the rotation matrix for the described transformation. Looking at the components of the metric tensor, h_{rr}, h_{rt} and h_{tt} transform as scalars,

$$\begin{cases} h'_{r'r'}(\theta',\varphi') = h_{rr}\left(\theta(\theta',\phi'),\varphi(\theta',\phi')\right); \\ h'_{t'r'}(\theta',\varphi') = h_{tr}\left(\theta(\theta',\phi'),\varphi(\theta',\phi')\right); \\ h'_{t't'}(\theta',\varphi') = h_{tt}\left(\theta(\theta',\phi'),\varphi(\theta',\phi')\right); \end{cases} \tag{4.15}$$

While $h_{t\,a}$ and $h_{r\,a}$, for a going through θ and φ, transform as 2-vectors under rotation as,

$$\begin{cases} h'_{r'\,a'}(\theta',\varphi') = R^a_{a'}\left(\hat{\mathbf{n}},\hat{\phi}\right)h_{ra}\left(\theta(\theta',\phi'),\varphi(\theta',\phi')\right); \\ h'_{t'\,a'}(\theta',\varphi') = R^a_{a'}\left(\hat{\mathbf{n}},\hat{\phi}\right)h_{ta}\left(\theta(\theta',\phi'),\varphi(\theta',\phi')\right). \end{cases} \tag{4.16}$$

Finally, the remaining components, $h_{a,b}$ for $a,b \in \{\theta,\varphi\}$, transform as a tensor,

$$h'_{a'\,b'}(\theta',\varphi') = R^a_{a'}\left(\hat{\mathbf{n}},\hat{\phi}\right)R^b_{b'}\left(\hat{\mathbf{n}},\hat{\phi}\right)h_{ab}\left(\theta(\theta',\phi'),\varphi(\theta',\phi')\right). \tag{4.17}$$

A construction of these components can be made in terms of spherical harmonics (Regge; Wheeler, 1957; Zerilli, 1970). For the scalars their angular part is simply proportional to a spherical harmonic,

$$\Phi^{(\mathrm{S})}_{\ell m} = c_{\ell m}Y_{\ell m}(\theta,\varphi). \tag{4.18}$$

Similarly, two types of vectors can be constructed as,

$$\Psi^{(\mathrm{V})}_{\ell m a} = c_{\ell m}\partial_a Y_{\ell m}(\theta,\varphi); \tag{4.19}$$

$$\Phi^{(\mathrm{V})}_{\ell m a} = c_{\ell m}\gamma^{bd}\epsilon_{ab}\partial_d Y_{\ell m}(\theta,\varphi); \tag{4.20}$$

with γ^{ab} being the contravariant metric tensor of the 2-sphere and ϵ_{bd} the permutation signal. At last, three types of tensor can be generated by this procedure,

$$\Psi^{(\mathrm{T})}_{\ell m ab} = c_{\ell m}\nabla_a\nabla_b Y_{\ell m}(\theta,\varphi); \tag{4.21}$$

$$\Phi^{(\mathrm{T})}_{\ell m ab} = c_{\ell m}\gamma_{ab}Y_{\ell m}(\theta,\varphi); \tag{4.22}$$

$$\chi^{(\mathrm{T})}_{\ell m ab} = \frac{1}{2}c_{\ell m}\gamma^{df}\left[\epsilon_{af}\nabla_d\nabla_b Y_{\ell m}(\theta,\varphi) + \epsilon_{bf}\nabla_d\nabla_a Y_{\ell m}(\theta,\varphi)\right]; \tag{4.23}$$

with ∇_a being the covariant derivative in the 2-sphere.

A second relevant symmetry to investigate is how this tensor and its components transform under spatial inversion, i.e., its parity. This transformation is given by $(\theta,\phi) \to$

$(\pi-\theta, \pi+\phi)$ and affects these quantities by multiplying $\Phi^{(\mathrm{V})}_{\ell m a}$ and $\chi^{(\mathrm{T})}_{\ell m a b}$ by a signal of $(-1)^{\ell+1}$ and the others by $(-1)^{\ell}$. As a spherically symmetric background metric is invariant under inversion, no mixing occurs between the two types of parity and the metric can be separated into two components(Chandrasekhar, 1984; Regge; Wheeler, 1957): axial, transforming as $(-1)^{\ell+1}$,

$$h^{(\mathrm{axial})}_{\mu\nu} = \begin{bmatrix} 0 & 0 & h_0(t,r)\Phi^{(\mathrm{V})}_{lm\,\theta} & h_0(t,r)\Phi^{(\mathrm{V})}_{lm\,\varphi} \\ 0 & 0 & h_1(t,r)\Phi^{(\mathrm{V})}_{lm\,\theta} & h_1(t,r)\Phi^{(\mathrm{V})}_{lm\,\varphi} \\ " & " & h_2(t,r)\chi^{(\mathrm{T})}_{\ell m\theta\theta} & h_2(t,r)\chi^{(\mathrm{T})}_{\ell m\theta\varphi} \\ " & " & " & h_2(t,r)\chi^{(\mathrm{T})}_{\ell m\varphi\varphi} \end{bmatrix}, \tag{4.24}$$

and polar, which transform as $(-1)^{\ell}$.

$$h^{(\mathrm{polar})}_{\mu\nu} = \begin{bmatrix} H_0(t,r)\Phi^{(\mathrm{S})}_{\ell m} & H_1(t,r)\Phi^{(\mathrm{S})}_{\ell m} & V_0(t,r)\Psi^{(\mathrm{V})}_{lm\,\theta} & V_0(t,r)\Psi^{(\mathrm{V})}_{lm\,\varphi} \\ " & H_2(t,r)\Phi^{(\mathrm{S})}_{\ell m} & V_1(t,r)\Psi^{(\mathrm{V})}_{lm\,\theta} & V_1(t,r)\Psi^{(\mathrm{V})}_{lm\,\varphi} \\ " & " & K(t,r)\Psi^{(\mathrm{T})}_{\ell m\theta\theta} + G(r,t)\Phi^{(\mathrm{T})}_{\ell m\theta\theta} & K(t,r)\Psi^{(\mathrm{T})}_{\ell m\theta\varphi} + G(r,t)\Phi^{(\mathrm{T})}_{\ell m\theta\varphi} \\ " & " & " & K(t,r)\Psi^{(\mathrm{T})}_{\ell m\varphi\varphi} + G(r,t)\Phi^{(\mathrm{T})}_{\ell m\varphi\varphi} \end{bmatrix} \tag{4.25}$$

A similar argument can be applied to the Electromagnetic Potential by first observing that the components A^t and A^r transform as scalars and A^θ and A^ϕ form together a 2-Vector. In this manner, A^μ can be separated into its axial and polar components,

$$A^{\mu(1)}_{\mathrm{axial}} = A_0(t,r)\left[0, 0, \Psi^{(\mathrm{V})}_{lm\,\theta}, \Psi^{(\mathrm{V})}_{lm\,\varphi}\right]; \tag{4.26}$$

$$A^{\mu(1)}_{\mathrm{polar}} = \left[A_1(t,r)\Phi^{(\mathrm{S})}_{\ell m}, A_2(t,r)\Phi^{(\mathrm{S})}_{\ell m}, A_3(t,r)\Phi^{(\mathrm{V})}_{lm\,\theta}, A_3(t,r)\Psi^{(\mathrm{V})}_{lm\,\varphi}\right]. \tag{4.27}$$

A further simplification is achieved by fixing a gauge for these two perturbations. In electromagnetism a simplifying choice would be the Coulomb Gauge $A^0 = 0$ reducing the potential to three independent functions. As for gravity, Regge and Wheeler propose a gauge that eliminates the h_2 component for the axial case and that eliminates V_0, V_1, and G in the polar one (Regge; Wheeler, 1957).

Besides the numerical simplification provided by separating these equations into their scalar, vector and tensor components, these components might aid in the physical intuition of the perturbation. On a FLRW metric, for example, the scalar components are tied to over- and under-densities in the mass distribution across the cosmos, while tensor perturbations provide the gravitational wave background (Dodelson; Schmidt, 2020; Weinberg, 2008).

As for axisymmetric spacetimes in prolate spheroidal coordinates, the transformation under rotation still separates the fields into the aforementioned three types of

components. However, there will be a mixing of different spherical harmonics, as the linearized equations now have an explicit dependence in $y = \cos(\theta)$. Moreover, in general, an axisymmetric object does not have to be invariant under spatial inversion, which could lead to a mixing of axial and polar modes, even though the studied Gutsunaev-Manko's metric is. This is easily verifiable by checking that the metric coefficients have only a squared dependence in y, and thus are not altered by inversion, given by $(y, \varphi) \to (-y, \pi + \varphi)$ in this coordinate system.

Finally, external fields can also be classified by how they transform under rotations, namely, by their spin. Spin-0 fields are scalars field: they might be charged or uncharged, are described by the Klein-Gordon equation, and either represent bosonic fields such as pions or the Higgs, or serve as classical limit of some matter fields. Spin-1/2 fields are fermionic fields: they are described by the Dirac Equation and represent fermions, such as electrons, muons, or neutrinos. At last, spin-1 fields are vector fields: they are described by a Proca equation and can represent either the electromagnetic field or the massive vector bosons, Z and W, that mediate the weak interaction.

4.2 Uncharged Scalar Fields

The simplest test case for a perturbative matter field is to introduce a uncharged scalar field. Such a field is described by a mapping from the Spacetime manifold to the Real numbers, $\Psi : \mathcal{M}[g_{\mu\nu}] \to \mathbb{R}$, which is minimally coupled to gravity as described by the action,

$$S = -\frac{1}{2}\int d^4x\,\sqrt{-g}\,\left[g^{\mu\nu}(\nabla_\mu\Psi)(\nabla_\nu\Psi) + m^2\Psi^2\right]. \tag{4.28}$$

Extremizing this action leads to the Covariant Klein-Gordon Equation (Wald, 1995),

$$\nabla_\mu\nabla^\mu\Psi - m^2\Psi = 0. \tag{4.29}$$

Equation (4.29) represents a massive field without self-interactions. However, the mass term will act as a positive linear term to an effective potential of this field. As a result, an increase in mass will lead to a higher stability of the field going against the proposed intention of finding unstable behavior around Gutsunaev-Manko's solution. Treating the field as massless is, nevertheless, sensible if the field's kinetic or gravitational energy is sufficiently larger than its rest energy, the latter being true for matter distributions in the neighbourhood of compact objects. Thus, the scalar perturbations are further on considered massless.

The D'Alambertian can be written purely in terms of the metric tensor and its determinant which leads to,

$$\frac{1}{\sqrt{g}}\partial_\mu\left(\sqrt{g}\, g^{\mu\nu}\partial_\nu\Psi\right) = 0, \tag{4.30}$$

which can be further expanded in terms of the metric functions f and g for the chosen gauge,

$$-\partial_t^2\Psi + \frac{(x-1)f^4}{(x+1)^3 g^2}\left(\partial_x(x^2-1)\partial_x\Psi + \partial_y(1-y^2)\partial_y\Psi + \frac{g^2}{1-y^2}\partial_\phi^2\Psi\right) = 0. \tag{4.31}$$

Introducing a change of variables for the field,

$$\Psi = \frac{\psi}{x+1}, \tag{4.32}$$

allows the x derivative to be rewritten as,

$$\frac{1}{x+1}\partial_x(x^2-1)\partial_x\Psi = \partial_x\left(\frac{x-1}{x+1}\right)\partial_x\psi - \frac{2\psi}{(x+1)^3}. \tag{4.33}$$

Thus, the wave equation in terms of the new variable is

$$-\partial_t^2\psi + \left(\frac{x-1}{x+1}\right)\frac{f^4}{g^2}\left(\partial_x\left(\frac{x-1}{x+1}\right)\partial_x\psi + \frac{1}{(x+1)^2}\left(\partial_y(1-y^2)\partial_y\psi + \frac{g^2}{(1-y^2)}\partial_\phi^2\psi - \frac{2\psi}{x+1}\right)\right) = 0. \tag{4.34}$$

In equation (4.34) the x derivative operator has the form

$$\frac{x-1}{x+1}\partial_x\frac{x-1}{x+1}\partial_x. \tag{4.35}$$

This motivates the transformation of the coordinate x to a new coordinate defined by its derivative as,

$$\partial_{\tilde{x}} = \frac{x-1}{x+1}\partial_x, \tag{4.36}$$

called a Tortoise Coordinate. An explicit transformation from the original radial prolate coordinate is given by $\tilde{x} = x + 2\,\ln(x-1)$. This is exactly the same tortoise coordinate as defined for a Schwarzschild Black Hole and in both cases it maps the horizon at $x = 1$ to $\tilde{x} \to -\infty$. The name tortoise coordinate is, thus, an allusion to Zeno's Paradox, as the coordinates come ever closer to the horizon without ever reaching it.

In the original Schwarzschild case this transformation also introduced the benefit of relaxing the need for a complicated boundary condition at the event horizon. However, in Gutsunaev-Manko's case the existence of naked singularities demand the imposition of further boundary conditions to cover them. As such, this transformation serves primarily for the algebraic convenience it provides in this scenario.

Thus, by applying the tortoise coordinate, the wave equation becomes,

$$-\partial_t^2\psi + \frac{f^4}{g^2}\left(\partial_{\tilde{x}}^2\psi + \frac{x-1}{(x+1)^3}\left(\partial_y(1-y^2)\partial_y\psi + \frac{g^2}{1-y^2}\partial_\phi^2\psi - \frac{2\psi}{x+1}\right)\right) = 0. \tag{4.37}$$

4.2.1 Spherical Harmonics Decomposition

To further tackle the solution of equation (4.37), it is worth introducing the Spherical Harmonics, $Y_l^m(\theta,\phi)$. These are functions defined by the property of being auto-functions of the angular part of the Laplace operator, i.e.,

$$\left[\frac{1}{\sin\theta}\partial_\theta\ (\sin\theta\,\partial_\theta) + \frac{1}{\sin^2\theta}\partial_\phi^2\right] Y_\ell^m(\theta,\phi) = -\ell(\ell+1)Y_\ell^m(\theta,\phi), \tag{4.38}$$

which in terms of the prolate spheroidal coordinate, $y = \cos\theta$, becomes

$$\left(\partial_y(1-y^2)\partial_y + \frac{1}{1-y^2}\partial_\phi^2\right) Y_\ell^m(y,\phi) = -\ell(\ell+1)Y_\ell^m(y,\phi). \tag{4.39}$$

The functions form a basis for the space of functions of $(y,\phi) \in [-1,1]\times[0,2\pi] \subset \mathbb{R}^2$, which can be made orthogonal by,

$$\left\langle Y_\ell^m, Y_{\ell'}^{m'}\right\rangle = \int_{-1}^{1}\int_0^{2\pi} Y_\ell^m(y,\phi)\bar{Y}_{\ell'}^{m'}(y,\phi)d\phi dy = \delta_{\ell\ell'}\delta_{mm'}. \tag{4.40}$$

A canonical description of the Spherical Harmonics is given in terms of the Associated Legendre Polynomials as,

$$Y_l^m(y,\phi) = \sqrt{\frac{2\ell+1}{4\pi}\frac{(l-m)!}{(l+m)!}}\,P_l^m(y)\,e^{im\phi}, \tag{4.41}$$

while the polynomials themselves are,

$$P_l^m(y) = \frac{(-1)^m(1-y^2)^{m/2}}{2^\ell\,\ell!}\frac{d^{\ell+m}}{dy^{\ell+m}}\left(y^2-1\right)^\ell. \tag{4.42}$$

It is worth noting that the inner product between these polynomials is diagonal in m, i.e.,

$$< P_\ell^m, P_{\ell'}^{m'} >= c_{\ell\ell'}\delta_{mm'}. \tag{4.43}$$

Given that, the scalar field is expanded in terms of the Spherical Harmonics,

$$\psi(t,\tilde{x},y,\phi) = \sum_{\ell m} u_{\ell m}(t,\tilde{x})Y_\ell^m(y,\phi), \tag{4.44}$$

which substituted into the wave equation leads to,

$$-\sum_{\ell,m} Y_\ell^m\partial_t^2 u_{\ell m} + \sum_{\ell,m}\frac{f^4}{g^2}\left(Y_\ell^m\partial_{\tilde{x}}^2 u_{\ell m} - \frac{x-1}{(x+1)^3}\left(\ell(\ell+1) + \frac{m^2(g^2-1)}{1-y^2} + \frac{2}{x+1}\right)Y_\ell^m u_{\ell m}\right) = 0. \tag{4.45}$$

Finally, equation (4.45) is multiplied by $Y_{\ell'}^{m'}$, and then integrated with respect to y and ϕ. The independence of the metric coefficients in ϕ and the diagonality of the

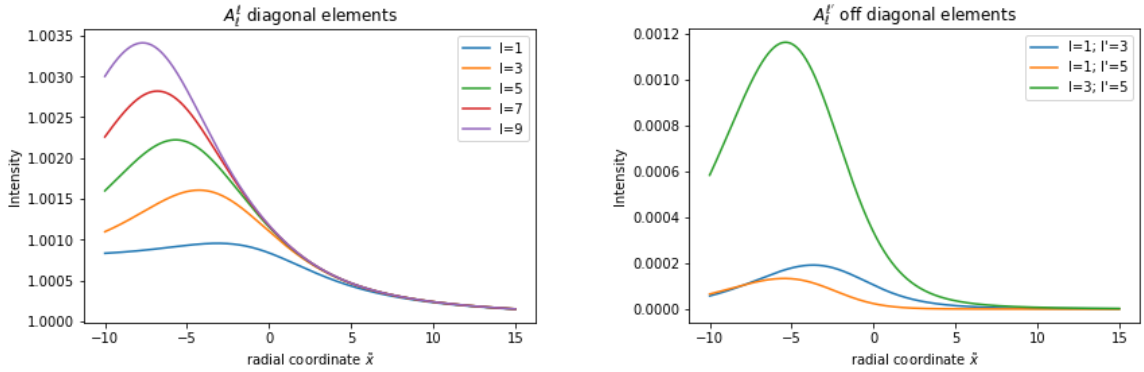

(a) Diagonal elements (b) Off diagonal elements

Figure 5 – Refraction index matrix of a scalar field, A_ℓ^k, for $m = 1$ and $\alpha = 10^{-2}$ in tortoise coordinates.

Associated Legendre Polynomials in m, as shown in equation (4.43), leads to a collection of matrix differential equations,

$$-\partial_t^2 u_{\ell m} + \sum_{\ell'} A_\ell^{\ell'} \partial_{\tilde{x}}^2 u_{\ell' m} = \sum_{\ell'} B_\ell^{\ell'} u_{\ell' m}, \tag{4.46}$$

with

$$A_\ell^{\ell'} = \left\langle Y_\ell^m, \frac{f^4}{g^2} Y_{\ell'}^m \right\rangle, \tag{4.47}$$

corresponding to a coupling to the kinetic energy of the other modes and

$$B_\ell^{\ell'} = \frac{x-1}{(x+1)^3} \left(A_\ell^{\ell'} V_{\text{eff}} + m^2 \left\langle Y_\ell^m, \frac{g^2-1}{1-y^2} \frac{f^4}{g^2} Y_{\ell'}^m \right\rangle \right), \tag{4.48}$$

corresponding to the self-interaction potential of each mode for $\ell = \ell'$ and a interaction potential between modes, otherwise. Lastly, the effective potential, V_{eff}, is given by,

$$V_{\text{eff}} = \ell(\ell+1) + \frac{2}{x+1}. \tag{4.49}$$

In the Schwarzschild limit the functions f and g become constant and equal to one and, thus, the $A_\ell^{\ell'}$ matrix will simplify to the Identity. As for the matrix $B_\ell^{\ell'}$, the term dependent on the inner product will vanish reducing it to a diagonal matrix of the form,

$$B_\ell^{\ell'}\Big|_{\alpha=0} = \frac{x-1}{(x+1)} \left(\frac{\ell(\ell+1)}{(x+1)^2} + \frac{2}{(x+1)^3} \right) \delta_l^{l'} = \left(1 - \frac{2}{r}\right) \left(\frac{\ell(\ell+1)}{r^2} + \frac{2}{r^3} \right) \delta_l^{l'}, \tag{4.50}$$

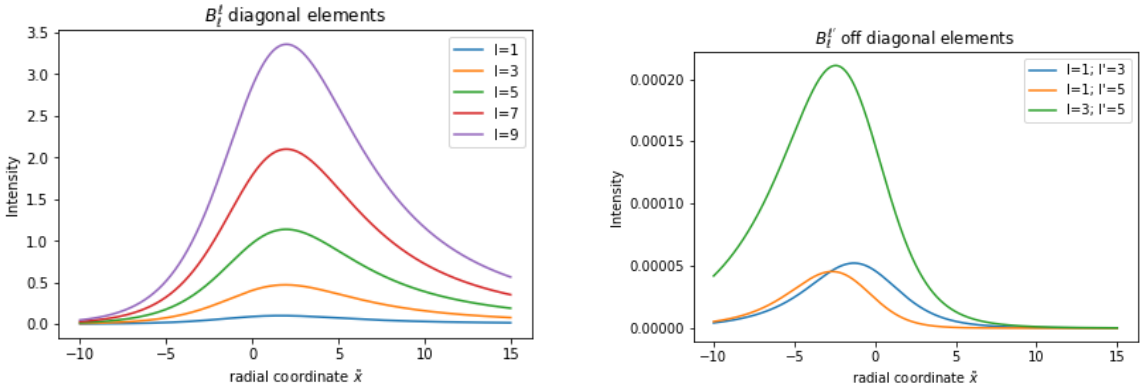

(a) Diagonal elements (b) Off-diagonal elements

Figure 6 – Potential matrix of an uncharged scalar field, B_ℓ^k, for $m = 1$ and $\alpha = 10^{-2}$ in tortoise coordinates.

which is exactly the Regge-Wheeler potential (Kokkotas, 1999; Regge; Wheeler, 1957) for a scalar perturbation of the Schwarzschild Black Hole.

It is also worth noting that for g, as described in equation (3.50), the limit

$$\lim_{y\to 1^+} \frac{g^2-1}{1-y^2} = 1 \tag{4.51}$$

is well defined. This means that the integration performed in equation (4.48) converges for every combination of ℓ and ℓ' outside the region containing the singularity.

Finally, the equations defined by (4.46) are all hyperbolic in the region of interest and of second-order. This means that a solution can be evolved by describing the configuration of the field in an initial Cauchy Domain (Wald, 1984; Baumgarten; Shapiro, 2010), which for the Weyl Gauge can be a closed region of the real line for the prolate radial coordinate, x, for a fixed time, alongside the time derivative of the field in this domain.

4.3 Charged Scalar Fields

Despite its simplicity, an uncharged field interacts with the compact object only through gravity. In this scenario all effects from the introduction of a non-perturbative magnetic dipole field to the metric, which differentiates it from the limiting Schwarzschild case, are only felt by the superimposed scalar field in terms of their deformation of spacetime. Thus, a charged field which can interact directly with the electromagnetic field is considered.

To upgrade the scalar field to a charged one, one first considers a complex field given by a mapping from the spacetime manifold to the Complex numbers, $\Psi : \mathcal{M}[g_{\mu\nu}] \to \mathbb{C}$, with an action,

$$S = -\frac{1}{2}\int d^4x\,\sqrt{-g}\,\left[g^{\mu\nu}(\nabla_\mu\Psi^*)(\nabla_\nu\Psi) + m^2\Psi^*\Psi\right]. \tag{4.52}$$

As it is currently stated, equation (4.52) is not different from the Lagrangian of two uncharged scalar fields with the same mass m by a simple decomposition of its real and imaginary parts as $\Psi = \psi_1 + i\psi_2$. In its form this field presents a global U(1) gauge invariance as the transformation $\Psi \mapsto e^{iq\alpha}\Psi$, for real constants α and q, preserves the action. However, motivated by the gauge invariance of the electromagnetic field, a local gauge invariance is imposed by transforming the field as $\Psi \mapsto U_q(x)\Psi$ with $U_q(x) = e^{iq\alpha(x)}$ being an element of U(1) and q defined to be the charge density of the field. If the Lagrangian is required to be invariant by this symmetry, it leads to,

$$\begin{aligned} S' &= -\frac{1}{2}\int d^4x\,\sqrt{-g}\,\left[g^{\mu\nu}\left(\nabla_\mu(U_q^\dagger\Psi^*)\right)\left(\nabla_\nu(U_q\Psi)\right) + m^2U_q^\dagger\Psi^*U_q\Psi\right] \\ &= -\frac{1}{2}\int d^4x\,\sqrt{-g}\,\{g^{\mu\nu}\left[\left(\nabla_\mu\Psi^*\right)\left(\nabla_\nu\Psi\right) - iq\left(\left(\nabla_\mu\alpha\right)\Psi^*\left(\nabla_\nu\Psi\right) - \left(\nabla_\nu\alpha\right)\Psi\left(\nabla_\mu\Psi^*\right)\right)\right. \\ &\quad \left. ... + q^2(\nabla_\nu\alpha)(\nabla_\mu\alpha)\Psi^*\Psi\right] + m^2\Psi^*\Psi\Big\}. \end{aligned} \tag{4.53}$$

From Noether's theorem the second term in equation (4.53) can be identified as a current,

$$j_\mu = iq\left[\Psi^*\left(\nabla_\mu\Psi\right) - \Psi\left(\nabla_\mu\Psi^*\right)\right], \tag{4.54}$$

with an associated conserved charge,

$$Q = iq\int d^3x j^0 = iq\int d^3x\left[\Psi^*\left(\nabla^0\Psi\right) - \Psi\left(\nabla^0\Psi^*\right)\right]. \tag{4.55}$$

Thus, the demand for this symmetry introduced a vector field B_μ, which should transform under a gauge symmetry as $B'_\mu = B_\mu + \partial_\mu\alpha$. In order for this field to also propagate, a kinetic term should be added. It should be the contraction of a tensor formed by the covariant derivative with the contravariant version of this tensor. To preserve Lorenz invariance, these tensors should be created from either symmetric or anti-symmetric vectors. The anti-symmetric one is,

$$F_{\mu\nu} = \nabla_\mu B_\nu - \nabla_\nu B_\mu, \tag{4.56}$$

Which is equivalent to the Electromagnetic Tensor and as such is manifestly invariant under the gauge transformations required by the electromagnetic potential. The symmetric tensor, conversely, would be,

$$G_{\mu\nu} = \nabla_\mu B_\nu + \nabla_\nu B_\mu. \tag{4.57}$$

This tensor, however, is not invariant under these gauge transformations. Nevertheless, as gauge transformations are required for quantization (Maggiore, 2005), this term should be discarded for the representation of a field theory in curved space. Consequently,

one is left with an extra field that behaves exactly as the electromagnetic field coupled to a matter field allowing the new variable B_μ to be identified with the electromagnetic potential A_μ. This corresponds to the Proca action, which also includes a mass term $m_\gamma^2 A_\mu A^\mu$. However, photons are supposed to either be massless or have vanishingly small masses for the lengths involved in this problem (Ryutov, 2007). This term will be left out.

The full Lagrangian for the background with the perturbative charged scalar field can, therefore, be written as,

$$\begin{aligned} S = \int d^4x \sqrt{-g}\, \{R - \frac{1}{4}F_{\mu\nu}F^{\mu\nu} \\ - \frac{1}{2}\left[(\nabla_\mu \Psi^*)(\nabla^\mu \Psi) - A_\mu j^\mu + \left(m^2 + q^2 A_\mu A^\mu\right)\Psi^*\Psi\right]\}. \end{aligned} \tag{4.58}$$

Applying the variational principle to the electromagnetic field in equation (4.58) leads to equation (4.6), while applying it to Ψ and introducing the gauge covariant derivative, $D_\mu = \nabla_\mu - iqA_\mu$, leads to the Klein-Gordon equation with an electric interaction,

$$\left(D_\mu D^\mu + m^2\right)\Psi = \left[\nabla_\mu \nabla^\mu + 2iqA^\mu \nabla_\mu + iq(\nabla_\mu A^\mu) - q^2 A_\mu A^\mu + m^2\right]\Psi = 0. \tag{4.59}$$

As the background field was derived in the Lorenz gauge, i.e., $\nabla_\mu A^\mu = 0$ and if the mass is equal to zero, the equation simplifies to,

$$\nabla_\mu \nabla^\mu \Psi + 2iqA^\mu \nabla_\mu \Psi - q^2 A_\mu A^\mu \Psi = 0, \tag{4.60}$$

If one applies the identity for the covariant derivative in terms of the metric tensor and its determinant,

$$\nabla_\mu \nabla^\mu \Psi = \frac{1}{\sqrt{-g}}\partial_\mu(\sqrt{-g}g^{\mu\nu}\partial_\nu \Psi), \tag{4.61}$$

together with the fact that the covariant derivative of a scalar is simply the directional derivative, the Klein-Gordon equation becomes,

$$\frac{1}{\sqrt{-g}}\partial_\mu(\sqrt{-g}g^{\mu\nu}\partial_\nu \Psi) + 2iqA^\mu \partial_\mu \Psi - q^2 A_\mu A^\mu \Psi = 0. \tag{4.62}$$

The whole equation is subsequently multiplied by the metric determinant, $\sqrt{-g}$, and opened in terms of its components, such that one arrives at the charged analogue of equation (4.31),

$$\begin{aligned} -\partial_t^2 \Psi + \frac{(x-1)f^4}{(x+1)^3 g^2}\left(\partial_x(x^2-1)\partial_x \Psi + \partial_y(1-y^2)\partial_y \Psi + \frac{g^2}{1-y^2}\partial_\varphi^2 \Psi\right) \\ + 2iqA_\varphi \frac{g^{\varphi\varphi}}{g^{tt}}\sqrt{-g}\partial_\varphi \Psi - q^2 A_\varphi A_\varphi \frac{g^{\varphi\varphi}}{g^{tt}}\sqrt{-g}\Psi = 0. \end{aligned} \tag{4.63}$$

Aside from being complex valued, equation (4.63) differs from its uncharged equivalent by the presence of the two last terms,

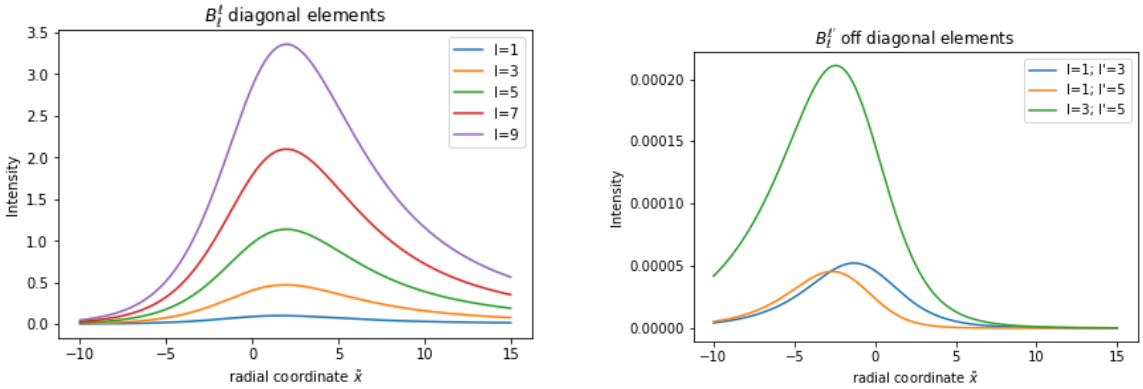

(a) Diagonal elements (b) Off diagonal elements

Figure 7 – Total potential matrix of a charged scalar field, B_ℓ^k, for $m = 1$, $q = -1$ and $\alpha = 10^{-2}$ in tortoise coordinates

$$\frac{-g^2 f^2 (x-1)}{(x+1)^2(1-y^2)} \left(2iqA_\varphi \partial_\varphi \psi - q^2 A_\varphi A_\varphi \psi\right), \tag{4.64}$$

in which the transformation $\Psi = \psi/(x+1)$. If the partial wave decomposition is introduced again, the derivative in φ becomes $\partial_\varphi Y_\ell^m = imY_\ell^m$, leading to

$$\frac{g^2 f^2 (x-1)}{(x+1)^2(1-y^2)} \left(2qmA_\varphi + q^2 A_\varphi^2\right) u_{\ell,m} Y_\ell^m, \tag{4.65}$$

which can be seen as a real valued potential term. Thus, the potential matrix defined in equation (4.48) is adapted as

$$B_\ell^{\ell'} = \frac{x-1}{(x+1)^3} \left(A_\ell^{\ell'} V_{\text{eff}} + m^2 \left\langle Y_\ell^m, \frac{g^2-1}{1-y^2} \frac{f^4}{g^2} Y_{\ell'}^m \right\rangle \right) + C_\ell^{\ell'}, \tag{4.66}$$

with $C_\ell^{\ell'}$ being

$$C_\ell^{\ell'} = \frac{x-1}{(x+1)^2} \left\langle Y_\ell^m, \frac{g^2 f^2}{(1-y^2)} \left(2qmA_\varphi + q^2 A_\varphi^2\right) Y_{\ell'}^{m'} \right\rangle. \tag{4.67}$$

4.4 Boundaries and Star Solutions

In (stationary) Black Hole solutions, the region outside the event horizon is causally disconnected from the region inside. This behavior can be captured by the tortoise coordinates, as the evolution for any finite time interval Δt of a finite region of space $(\tilde{a}, \tilde{b}) \subset \mathbb{R}$ is prescribed by the field's initial state in an also finite region of space $(\tilde{a}_0, \tilde{b}_0) \subset \mathbb{R}$. In turn, this is observed due to the ever-increasing redshift suffered by an infalling test particle as seen from an outside observer at infinity. In fact, for the regular region of Spacetime described by GM solution, such as the equatorial plane, this is the observed behavior as shown in equation (3.67).

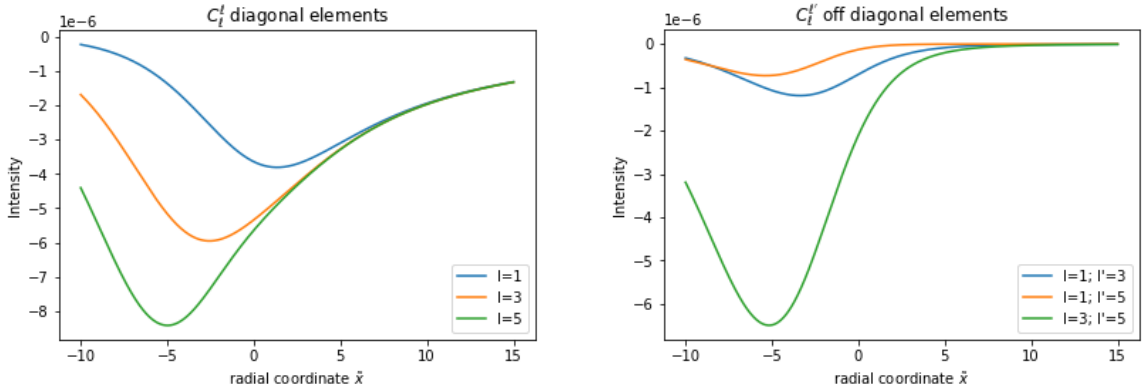

(a) Diagonal elements (b) Off diagonal elements

Figure 8 – Electromagnetic potential matrix of a charged scalar field, C_ℓ^k, for $m = 1$, $q = -1$ and $\alpha = 10^{-2}$ in tortoise coordinates

This procedure suppresses the need to deal with the incoming wave boundary condition in the horizon as it is specially difficult for numerical methods. However, the lack of a physical interpretation for the naked singularities in the studied metric means that there is not a reasonable definition for the field in the regions containing them.

A different approach is to introduce a star solution. By that the electrovacuum solution is supposed to describe the exterior of a gravitationally bound object, such as a star or a neutron star. The star then corresponds to a bounded region, $\Sigma_{\text{star}} \subset \mathbb{R}^3$, composed of a collection of matter fields, each described by their equation of state and that vanish outside of this region. Furthermore, the Einstein-Maxwell equations for the interior of Σ_{star} are demanded to be compatible with the vacuum metric outside, such as by demanding the continuity of the metric at the boundary $\partial\Sigma_{\text{star}}$.

While this approach has led to many different solutions (Zel'dovich, 1971) including the Tolman-Oppenheimer-Volkoff (Tolman, 1939; Oppenheimer; Volkoff, 1939) for a perfect fluid, finding an appropriate description to the equations of state of matter in the star's interior that can be fitted to the exterior metric is an intricate procedure and is further complicated by the requirement of a source for the magnetic field. Therefore, a simplification is made instead by considering the surface of the star impenetrable to the scalar field, thus, working as a mirror at a surface of constant x.

4.5 Normal and Quasi-Normal Modes

The equations presented so far for the wave propagation describe how it evolves over time for an initial perturbation. These are relevant in describing the waveforms of gravitational and electrical radiation resulting from astrophysical events, e.g., collisions between NS-NS, BH-BH, or NS-BH, as is used in experiments such as LIGO (Andersson; Kokkotas, 1998). However, in the search for explosive phenomena one wishes to study the

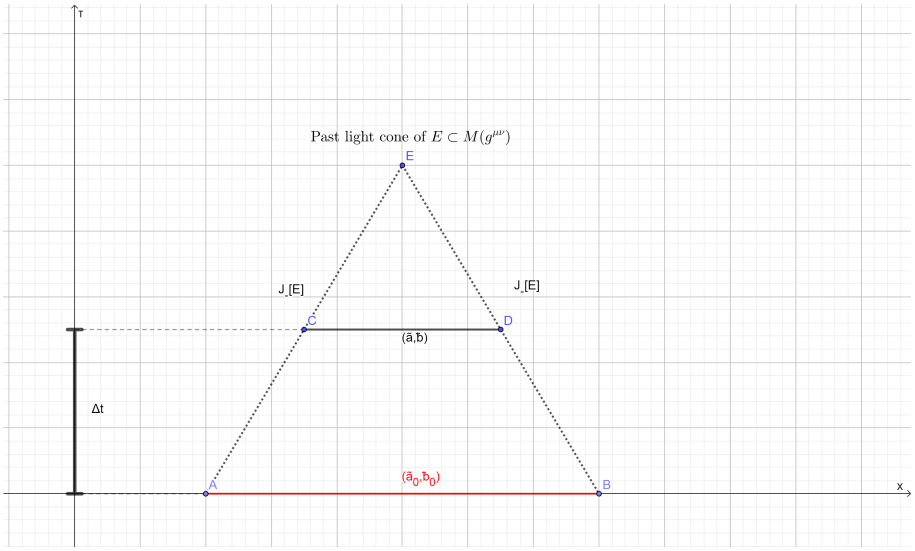

Figure 9 – Evolution of an initial Cauchy domain $(\tilde{a}_0, \tilde{b}_0)$ during a time Δt. The lines J_+ and J_- are null geodesics representing the boundaries of the hyperbolic domain, inside of which the causal domain of any point is a subset of the union of the causal domains of the points in the initial Cauchy domain. For these points the state of any field can be determined by the state of the field in the aforementioned region.

stability of the system. For that purpose one wishes to find if there are growing solutions in the linear model as time passes. Such a solution would represent the field gaining energy from the compact object and the background fields and has been described before for other metrics and types of fields (Penrose; Floyd, 1971; Zel'dovich, 1971; Starobinskiĭ, 1973; Baryakhtar et al., 2021). Of course, as the intensity increases, the validity of linear perturbation breaks down and higher-order terms, such as the back-reaction from gravitational and electromagnetic radiation, have to be calculated to derive the actual physical behavior.

In the case of propagation of a wave in an elastic material of finite size, such as in the vibration of a string fixed at each endpoint, the evolution of an initial excitation can be described in terms of a discrete set of frequencies. This can easily be seen by the Fourier transform of a one-dimensional wave equation,

$$\phi(x,t) = \tilde{\phi}(x,\omega)e^{i\omega t} \tag{4.68}$$

$$\omega^2\tilde{\phi} + \partial_x^2\tilde{\phi} = 0 \tag{4.69}$$

$$\tilde{\phi} = Ae^{i\omega x} + Be^{-i\omega x} = A'\cos(\omega x) + B'\sin(\omega x), \tag{4.70}$$

which, by imposing that ϕ vanishes at the extremities $a, b \in \mathbb{R}$ at all times, leads us to,

$$\omega_n = \frac{2\pi n}{b-a}, \text{ for } n \in \mathbb{N}. \tag{4.71}$$

Thus, the functions defined by $\tilde{\phi}_n$ for each frequency ω_n form an orthogonal basis over which the initial conditions can be decomposed, which leads to the time evolution in

terms of a Fourier Series,

$$\phi(x,t) = \sum_n \left[A_n \cos(\omega_n x) + B_n \sin(\omega_n x)\right] e^{i\omega_n t}; \tag{4.72}$$

$$A_n = \int_a^b \phi(x,0)\cos(\omega_n x)dx; \tag{4.73}$$

$$B_n = \int_a^b \phi(x,0)\sin(\omega_n x)dx. \tag{4.74}$$

For higher dimensional problems bound by a Dirichlet Boundary a discretized spectrum also appears.

In a dissipative medium a first order term is introduced in the equation leading the solution to be written in terms of a Laplace transformation. Here, the waves are decomposed in terms of a real frequency corresponding to the oscillating frequency as before and a imaginary frequency corresponding to a damping factor,

$$\phi = \tilde{\phi}(s,x)e^{st} = \tilde{\phi}(s,x)e^{i(\omega_{re}+i\omega_{im})t} = \tilde{\phi}(s,x)e^{i\omega_{re}t}e^{-\omega_{im}t}. \tag{4.75}$$

Once again, the imposition of a Dirichlet boundary at each end of the string would lead to the spectrum being discrete. Thus, due to forming a complete and orthogonal basis this type of modes are called normal modes.

A first intuition would, therefore, not indicate the existence of discrete modes for the perturbation of Black Holes: the potential being positive everywhere disallows the existence of bound states and, thus, we cannot impose the modes $\phi(s,x)$ to go to zero as x goes to the horizon or to infinity and, in fact, for a Minkowski space outside a spherical mirror this behaviour is not present. Yet, a damped mode-like behavior appears in the evolution of these perturbations (Regge; Wheeler, 1957; Vishveshwara, 1970) and extends also for oscillations around Neutron Stars (Andersson; Kokkotas, 1998) beyond the normal modes generated by the vibration of its matter contents in a framework of Newtonian gravity.

(a) Linear Scale (b) Log Scale

Figure 10 – Misner Waveform for a head-on collision of two Black HoleS. Image by (Nollert, 1999)

This oscillating behavior starts after some time of the initial excitation, until this time the behaviour is dominated by the initial conditions. In this period many modes

might be simultaneously excited, however, as time progresses, the modes with higher imaginary frequency die out leaving the slowly decaying modes. In the Schwarzschild geometry a single frequency oscillation can be observed for physically relevant setups, e.g., the ring-down from the head on collision of two Black Holes (Price; Pullin, 1994). At later times the evolution is finally dominated by a tail decreasing as power-law of the time passed since the initial excitation.

In contrast to the normal modes, however, these decaying solutions do not form a complete basis (Ching et al., 1996). Returning to the Schwarzschild case, the chosen boundary conditions lead to solutions that diverge at the horizon and at infinity and, thus, do not represent physical states on their own (Nollert, 1999). Thus, the initial condition cannot be fully decomposed in terms of them and this incompleteness lends them the name quasi-normal modes (QNM). In any case, in the region where the QNMs dominate the time dependence of the wave one can write the perturbative field as

$$\chi_n(t) = \sum_n c_n e^{i(\Omega^{(n)})t} = \sum_n c_n e^{i(\omega_{re}^{(n)} + i\omega_{im}^{(n)})t} = \sum_n c_n e^{i\omega_{re}^{(n)} t} \cdot e^{-\omega_{im}^{(n)} t}, \tag{4.76}$$

with a complex frequency $\Omega_n \in \mathbb{C}$, ordered by their imaginary part, i.e., how amortized they are, and c_n the relative intensity of each mode determined by how an initial condition would excite them.

While a more rigorous mathematical description of QNMs in terms of the Green's functions is given by (Andersson, 1997), intuition can be gained by the comparison of Fourier transformed wave equation to the Schrödinger Equation for resonant scattering (Sakurai; Napolitano, 2012). In this scenario the wave is momentarily trapped by the potential peak, which due to its finitude is not indefinitely bound. Thus, the wave slowly leaks out through the potential barrier.

In the final phase of the evolution, as the exponentially decaying QNM fades away, a power-law tail dominates (Price, 1972). This behavior is shown to originate from the inverse-square decay of the potential (Leaver, 1986; Ching et al., 1995), $V(r) \approx 1/r^2$ for large r, in contrast to the QNM behavior originated around the peak of the potential (Nollert, 1999). The waveform of this tail can be written as,

$$\chi_n(t) \propto t^{-(2\ell+P+1)}, \tag{4.77}$$

in which ℓ is the same as in the spherical harmonic and P is dependent on the initial data of the field. In specific, P = 1 if the initial field is stationary over a null surface, P = 3 if it is stationary over a Cauchy surface, and P = 2 if the observer is located at infinity (Nollert, 1999; Gundlach; Price; Pullin, 1994). The three phases of the wave evolution can be seen in figure 10.

While the linear perturbations for the Schwarzschild case were demonstrated to be stable (Vishveshwara, 1970; Regge; Wheeler, 1957), perturbations with increasing

amplitude were found for other metrics, such as the charged and static Reissner-Nordström (Benone; Crispino, 2016; Menza; Nicolas, 2015) or the rotating stationary Kerr Black Holes (Starobinskiĭ, 1973; Teukolsky; Press, 1974). In these cases the energy of the wave increases as it scatters around these objects, however, the amount gained is still bounded. A calculation of the back-reaction to the background black hole shows that the modes would cause them to lose their angular momentum or charge, respectively, and their mass. In turn, this accounts for the energy transferred to the perturbation (Brito; Cardoso; Pani, 2020). A gain of energy during the scattering of the perturbative wave in relation to the incoming weave is called superradiance, which is independent of the existence of a horizon, and can appear for stars. This phenomenon is a necessary condition for some known unstable modes of other geometries (Konoplya; Zhidenko, 2014) even if not sufficient, as there exists still superradiant stable modes.

5 Simulation and Results Analysis

The study of the perturbations on Black Holes and Stars has provided a set of equations for determining the time evolution of waves around these objects and how to infer their stability from its behavior. However, one is still left with solving them as even the wave equation for the Regge-Wheeler potential cannot be solved in a fully analytical form. For that purpose, some numerical and semi-analytical methods may be considered with a review of them having been compiled by Nollert (Nollert, 1999).

In the more analytical methods the Regge-Wheeler potential can be approximated by potentials with known solutions, such as a harmonic oscillator or a Pöschl-Teller potential. The potentials are fitted to the peak of the true potential and the corresponding frequencies are obtained (Ferrari; Mashhoon, 1984b; Ferrari; Mashhoon, 1984a). These, however, fail to approximate the modes with higher damping and longer wavelengths, as they have a stronger interaction with the potential away from its maximum.

The WKB approach, in turn, can also be appropriate to the calculation of QNM (Schutz; Will, 1985; Gal'tsov; Matiukhin, 1992; Konoplya; Zhidenko, 2011; Matyjasek; Opala, 2017; Matyjasek; Telecka, 2019). This method, originated in quantum mechanics, consists in approximating the function in different regions according to whether the wave's kinetic energy is higher than the potential's, i.e., the wave is in a propagating region, or if the converse is true, i.e., the wave is in a tunnelling region. In an one-dimensional propagation the time independent wave equation is

$$\frac{d^2\psi}{dx^2} + Q(x)\psi = 0, \tag{5.1}$$

with $Q(x) = [V(x) - \omega^2]$. The wave is thus approximated by a power series in its exponent and ψ and its first derivative are matched at the critical points, i.e., the roots of $Q(x)$. Moreover, the potential near the peak is approximated by a Taylor Series at the maximum of the potential in order to calculate ψ at the region where $Q(x) < 0$ (Konoplya; Zhidenko; Zinhailo, 2019; Konoplya; Zhidenko, 2022). Finally, the boundary conditions are imposed at positive and negative infinity and fulfilling these conditions and matching at the critical points determines the discretized oscillating frequencies.

This method is reliable for uni-dimensional potentials with a single maximum. However, as perturbations around a Gutsunaev-Manko's metric mix the different angular momenta, the equations cannot be reduced to the form expected in this method, and either a modification would have to be done to encompass it or deal with the two-dimensional problem in both prolate variables separating only the dependence in φ. Conversely, a numerical method, such as the Finite Difference method, provides a more general technique to estimate the QNMs at a higher computational cost.

5.1 Finite Differences

Finite differences is a numerical method for solving partial differential equations. It consists in approximating the derivatives by the difference of the function between two adjacent points and solving instead the algebraic equation (Baumgarten; Shapiro, 2010). In order to do this, first the integration domain of the differential equation, $[x_0, x_{\text{end}}] \times [t_0, t_{\text{end}}]$, is discretized into a grid of points of the form $(x_\ell, t_k) \equiv (x_0 + \Delta x \cdot \ell, t_0 + \Delta t \cdot k)$, with $k, \ell \in \mathbb{N}$, and the field is described at each point as $\psi(x_0 + \Delta x \cdot \ell, t_0 + \Delta t \cdot k) \equiv \psi_{\ell,k}$.

To calculate the derivatives, a Taylor series centered at each point of the grid is used to calculate the neighbouring points. Thus, truncating the coefficients at the order Δt^2,

$$\psi_{\ell,k+1} \equiv \psi(x_l, t_k + \Delta t) = \psi(x_l, t_k) + \frac{d\psi(x_l, t_k)}{dt}\Delta t + \frac{1}{2!}\frac{d^2\psi(x_l, t_k)}{dt^2}\Delta t^2 + O(\Delta t^3); \quad (5.2)$$

$$\psi_{\ell,k-1} \equiv \psi(x_l, t_k - \Delta t) = \psi(x_l, t_k) - \frac{d\psi(x_l, t_k)}{dt}\Delta t + \frac{1}{2!}\frac{d^2\psi(x_l, t_k)}{dt^2}\Delta t^2 + O(\Delta t^3). \quad (5.3)$$

If the two equations are added then terms with order higher than 2 in Δ are discarded, and the second derivatives isolated, this gives,

$$\ddot{\psi}_{\ell,k} \equiv \frac{d^2\psi(x_l, t_k)}{dt^2} = \frac{1}{\Delta t^2}\left(\psi_{\ell,k+1} - 2\psi_{\ell,k} - \psi_{\ell,k-1}\right). \quad (5.4)$$

By instead subtracting, the first derivative can be obtained,

$$\dot{\psi}_{\ell,k} \equiv \frac{d\psi(x_l, t_k)}{dt} = \frac{1}{\Delta t}\left(\psi_{\ell,k+1} - \psi_{\ell,k-1}\right). \quad (5.5)$$

While the time derivative was calculated at second order in the grid spacing, for the spatial derivative the fourth order is chosen in order to improve stability and accuracy of the numerical solution (Molina et al., 2004; Levander, 1988). At this order the neighbouring points are expanded as,

$$\psi_{\ell+2,k} = \psi(x_l, t_k) + \frac{d\psi(x_l, t_k)}{dx}(2\Delta x) + \frac{1}{2!}\frac{d^2\psi(x_l, t_k)}{dt^2}(2\Delta x)^2 + \frac{1}{3!}\frac{d^3\psi(x_l, t_k)}{dx^3}(2\Delta x)^3 + \frac{1}{4!}\frac{d^4\psi(x_l, t_k)}{dx^4}(2\Delta x)^4 + O(\Delta t^5); \quad (5.6)$$

$$\psi_{\ell+1,k} = \psi(x_l, t_k) + \frac{d\psi(x_l, t_k)}{dx}\Delta x + \frac{1}{2!}\frac{d^2\psi(x_l, t_k)}{dt^2}\Delta x^2 + \frac{1}{3!}\frac{d^3\psi(x_l, t_k)}{dx^3}\Delta x^3 + \frac{1}{4!}\frac{d^4\psi(x_l, t_k)}{dx^4}\Delta x^4 + O(\Delta t^5); \quad (5.7)$$

$$\psi_{\ell-1,k} = \psi(x_l, t_k) - \frac{d\psi(x_l, t_k)}{dx}\Delta x + \frac{1}{2!}\frac{d^2\psi(x_l, t_k)}{dt^2}\Delta x^2 - \frac{1}{3!}\frac{d^3\psi(x_l, t_k)}{dx^3}\Delta x^3 + \frac{1}{4!}\frac{d^4\psi(x_l, t_k)}{dx^4}\Delta x^4 + O(\Delta t^5); \quad (5.8)$$

$$\psi_{\ell-2,k} = \psi(x_l, t_k) - \frac{d\psi(x_l, t_k)}{dx}(2\Delta x) + \frac{1}{2!}\frac{d^2\psi(x_l, t_k)}{dt^2}(2\Delta x)^2 - \frac{1}{3!}\frac{d^3\psi(x_l, t_k)}{dx^3}(2\Delta x)^3 + \frac{1}{4!}\frac{d^4\psi(x_l, t_k)}{dx^4}(2\Delta x)^4 + O(\Delta t^5). \quad (5.9)$$

By defining $\Delta\psi_j \equiv \psi_{\ell,k+j} - \psi_{\ell,k}$, the above equations are written in matrix form,

$$\begin{pmatrix} -2 & 4 & -8 & -16 \\ -1 & 1 & -1 & 1 \\ 1 & 1 & 1 & 1 \\ 2 & 4 & 8 & 16 \end{pmatrix} \cdot \begin{pmatrix} \psi' \Delta x \\ \psi'' \frac{\Delta x^2}{2!} \\ \psi^{(3)} \frac{\Delta x^3}{3!} \\ \psi^{(4)} \frac{\Delta x^4}{4!} \end{pmatrix} = \begin{pmatrix} \Delta\psi_{-2} \\ \Delta\psi_{-1} \\ \Delta\psi_{+1} \\ \Delta\psi_{+2} \end{pmatrix}, \tag{5.10}$$

which can be easily solved as,

$$\begin{pmatrix} \psi' \Delta x \\ \psi'' \frac{\Delta x^2}{2!} \\ \psi^{(3)} \frac{\Delta x^3}{3!} \\ \psi^{(4)} \frac{\Delta x^4}{4!} \end{pmatrix} = \frac{1}{24} \begin{pmatrix} 2 & -16 & 16 & -2 \\ -1 & 16 & 16 & -1 \\ -2 & 8 & -8 & 2 \\ 1 & -8 & -8 & 1 \end{pmatrix} \cdot \begin{pmatrix} \Delta\psi_{-2} \\ \Delta\psi_{-1} \\ \Delta\psi_{+1} \\ \Delta\psi_{+2} \end{pmatrix}. \tag{5.11}$$

The coefficients for the $\psi_{\ell,k}$ term in the n-th derivative can be readily recovered by adding the terms of the corresponding row and multiplying by -1. Thus, at this accuracy level the second derivative is,

$$\psi''_{\ell,k} = \frac{1}{12(\Delta x)^2} \left(-\psi_{\ell-2,k} + 16\psi_{\ell-1,k} - 30\psi_{\ell,k} + 16\psi_{\ell+1,k} - \psi_{\ell+2,k}\right). \tag{5.12}$$

To avoid overloading the variables with indices and causing confusion between the integration grid indices and the angular momentum numbers, a vector notation for the partial wave decomposition is introduced as,

$$\bar{\psi} \equiv \begin{bmatrix} \psi_0 \\ \psi_1 \\ \psi_2 \\ \vdots \end{bmatrix}; \qquad \bar{A}\bar{\psi} \equiv \begin{bmatrix} \sum_{\ell'} A_0^{\ell'} \psi_{\ell'} \\ \sum_{\ell'} A_1^{\ell'} \psi_{\ell'} \\ \sum_{\ell'} A_2^{\ell'} \psi_{\ell'} \\ \vdots \end{bmatrix}. \tag{5.13}$$

In this notation equation (4.46) is written as,

$$-\partial_t^2 \bar{\psi} + \bar{A}\partial_x^2 \bar{\psi} = \bar{B}\bar{\psi}. \tag{5.14}$$

Finally, equations (5.4) and (5.12) are substituted into (5.14), which leads to the updated equation for the field at a point $(x_l, t_k + 1)$,

$$\bar{\psi_{\ell,t+1}} = 2\bar{\psi_{\ell,t}} - \bar{\psi_{\ell,t-1}} + \frac{\bar{A}}{12(\Delta x)^2} \left(-\psi_{\ell-2,k} + 16\psi_{\ell-1,k} - 30\psi_{\ell,k} + 16\psi_{\ell+1,k} - \psi_{\ell+2,k}\right) - \bar{B}\bar{\psi_{\ell,t}} \tag{5.15}$$

Thus, by specifying the values of the field over two consecutive instants of time, the grid can be propagated by calculating a matrix product and a convolution. These operations are particularly suited for computational implementation, even though grids of larger size can become computationally expensive.

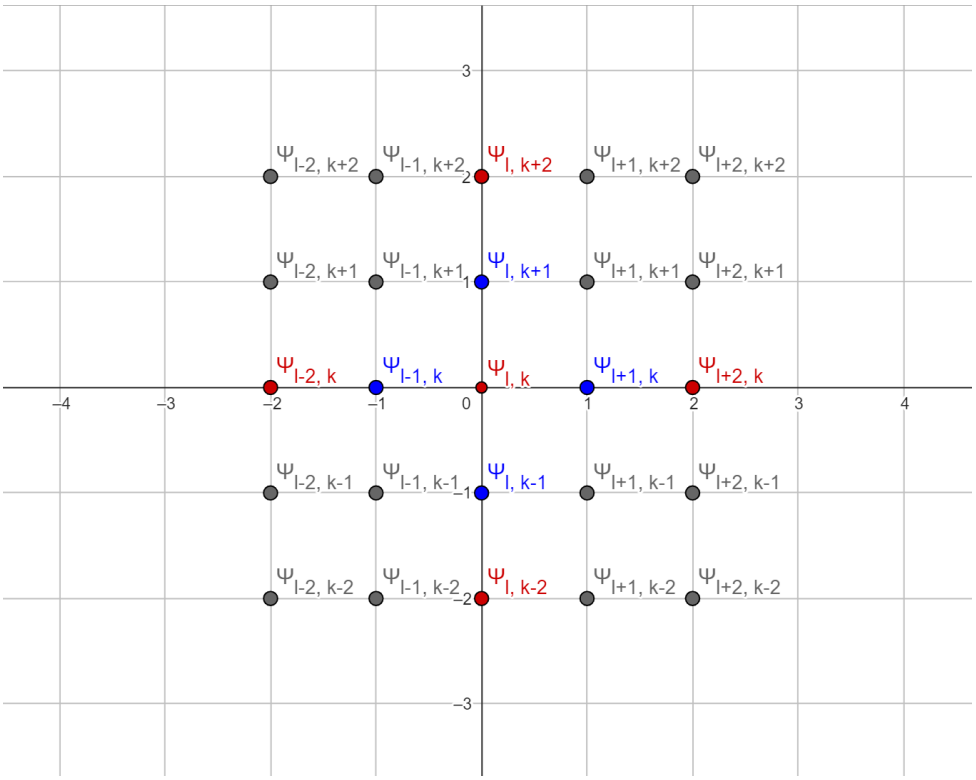

Figure 11 – Schema of the discretized space as a grid. Red (blue) dots represent the points that receive a negative (positive) coefficient in the discrete second order derivative with fourth order precision.

5.1.1 Boundary Conditions

On the limits of the grid the calculation from equation (5.15) cannot be performed, as the values of the field outside of the grid are undefined. As such, a choice must be made at this region on how to treat the evolution. If this boundary coincides with a physical boundary of the problem, over which the boundary conditions are stated, this reduces to implementing these conditions as a finite differences equation.

This is the case at the surface of the star with a perfectly reflective surface, for example, such as the one considered in this text. There, the condition of the field vanishing inside the star allows one to extend the grid inside it and impose the field to be null in these extra points in order to calculate the evolution of the points outside the star. If that is not the case, however, more care is needed. Any interaction of the wave with this region is unphysical, but rather an artifact of the numerical simulation, and should not be allowed to influence the parts of the field from which the results are being calculated. This might be the case, e.g., for terminating the grid on a finite value of an integration domain that extends to infinity. However, for a hyperbolic differential equation constraining the observed region to the causal domain of the initial conditions guarantees that the information from the unphysical borders of the grid have not had the time yet to propagate to these positions.

5.2 Numerical Setup

The setup used to obtain the QNMs for the metric consisted in simulating the time evolution of the partial waves by means of the finite difference method. The simulation was run with different parameters for α and $\tilde{x}_{min}$ with similar initial conditions.

The first step is to numerically integrate the internal product contained in matrices $A_\ell^{\ell'}$ and $B_\ell^{\ell'}$. This is done by using a Clenshaw-Curtis Curvature method integrator, implemented in python's Scipy.integrate library, at each point x of the discretized grid. The initial perturbation is then constructed by imposing a Gaussian wave profile with its peak after the potential peak. The next instant is approximated from the equation using a second order Taylor polynomial to generate the two points in time required by the second order equation.

The finite differences can then be performed by updating each point of the grid by using equation (5.15). The linear structure of this equation allows for optimized vectorial/tensorial implementations with python's Numpy library. In order for the grid not to overfill the RAM of the computer, the executing of the code is done in chunks of 2000 time steps after which the results are saved and the last two time points are used as new initial conditions.

Finally, once the simulation is finished, the modes are extracted by fitting an exponentially decaying cosine to the resulting waveform. The full evolution is truncated containing only the piece with the behavior we are interested in for the analysis, i.e., remove the initial conditions dependent part and the power-law tail. A pre-estimation is then performed by estimating the real frequency by the inverse average period, i.e., half the mean of the inverses of the time between two consecutive zeros of the wave. Similarly, the phase for the cosine is estimated by demanding the zeros to happen at the appropriate time. Lastly, the amplitude and the imaginary frequency are estimated by fitting a line to the log amplitude at the wave peaks. The results from this pre-estimation are passed as initial condition to a least-squares algorithm that fits the theoretical waveform of the data. The fitted wave is finally compared to the simulated one as a last check and if it passes, the resulting parameters are interpreted as the quasi normal frequencies.

5.3 Schwarzschild Limit

A first analysis of the simulation is the limit of a vanishing magnetic field. It corresponds to a Schwarzschild metric with a hard spherical shell, whose radius is greater than that of the horizon. By itself this presents little physical interest since the perturbation behavior of more realistic star models has been studied. Rather, this scenario presents a way to validate the results obtained by the simulation.

For the Schwarzschild geometry the metric functions f and g as defined in equation (3.48) become identically equal to 1. In turn, this implies that the matrices $A_\ell^{\ell'}$ and $B_\ell^{\ell'}$ become diagonal. While the presence of the spherical mirror shell will cause the QNM of this metric to differ from those of an uncharged static black hole, the lack of coupling between the different spherical harmonics enables the use of the semi-analytical methods, which were discarded in the magnetized case.

This has been done by (Ribeiro, 2024) based on a method by (Fiziev, 2005) and their method is outlined here. The time-independent wave equation for a single spherical harmonic, ℓ, is turned into a Confluent Heun Equation,

$$\frac{d^2U}{dz^2} + \left(\alpha + \frac{\beta}{z} + \frac{\gamma}{z-1}\right)\frac{dU}{dz} + \left(\frac{\mu}{z} + \frac{\nu}{z-1}\right)U = 0, \tag{5.16}$$

whose solution is named the Confluent Heun functions,

$$U(z) = HeunC(\alpha, \beta, \gamma, \delta, \eta; z). \tag{5.17}$$

There, the two final parameters are,

$$\mu = \frac{1}{2}(\alpha - \beta - \gamma + \alpha\beta - \beta\gamma) - \eta; \tag{5.18}$$

$$\nu = \frac{1}{2}(\alpha + \beta + \gamma + \alpha\gamma + \beta\gamma) + \delta + \eta. \tag{5.19}$$

To rewrite the wave equation in the appropriate form, the transformation to tortoise coordinates in the partial wave equation is not done, but rather the change of variables,

$$\xi = -\frac{x-1}{2}, \tag{5.20}$$

together with the transformation,

$$u_\ell(\xi) = \xi^{2im\omega} e^{2im\omega\xi}\omega_\ell(\xi) \tag{5.21}$$

is performed. This results in the equation,

$$\frac{d^2\omega_\ell}{d\xi^2} + \left(4im\omega + \frac{4im\omega+1}{\xi} + \frac{1}{\xi-1}\right)\frac{d\omega_\ell}{d\xi} + \left[\frac{4im\omega - \ell(\ell+1)}{\xi-1} + \frac{\ell(\ell+1) - 16m^2\omega^2}{\xi}\right]\omega_\ell = 0. \tag{5.22}$$

The parameters α, β, and γ are directly obtained by comparing equations (5.16) and (5.22), while η and δ are given by,

$$\delta = -8m^2\omega^2; \tag{5.23}$$

$$\eta = 8m^2\omega^2 - \ell(\ell+1). \tag{5.24}$$

Excited Mode ℓ	Mirror Position in turtle coordinates	Simulated ω_{re}	Simulated ω_{im}	Semi-analytical $\omega_{re}^{(a)}$	Semi-analytical $\omega_{im}^{(a)}$	Relative Difference $\Delta\omega_{re}\%$	Relative Difference $\Delta\omega_{im}\%$
3	-5	$6.517\quad 10^{-01}$	$7.248\quad 10^{-03}$	$6.513\quad 10^{-01}$	$7.277\quad 10^{-03}$	0.058	0.39
3	-3	$7.299\quad 10^{-01}$	$4.791\quad 10^{-02}$	$7.296\quad 10^{-01}$	$4.775\quad 10^{-02}$	0.038	0.33
1	-15	$2.117\quad 10^{-01}$	$7.49\quad 10^{-04}$	$2.116\quad 10^{-01}$	$7.46\quad 10^{-04}$	0.048	0.46
1	-10	$2.842\quad 10^{-01}$	$8.05\quad 10^{-03}$	$2.841\quad 10^{-01}$	$8.02\quad 10^{-03}$	0.050	0.31
1	-5	$3.717\quad 10^{-01}$	$6.78\quad 10^{-02}$	$3.703\quad 10^{-01}$	$6.69\quad 10^{-02}$	0.36	1.4

Table 1 – Comparison between results from the numerical simulation and the zeros from the Confluent Heun Functions for the Schwarzschild limit, i.e., when the magnetic field is null.

Mirror Position in tortoise coordinates	Simulated Power-law Coefficient	Relative Deviation from Schwarzschild
-5	-6.2	0.03
0.114	-6.2	0.03
0.578	-6.2	0.03
0.987	-6.2	0.03

Table 2 – Power-law coeficients for different mirror positions.

Finally, the general solution is given by,

$$\begin{aligned} u_\ell(\xi) = {} & C_1 \xi^{2im\omega} e^{2im\omega\xi} HeunC(4im\omega, 4im\omega, 0, -8m^2\omega^2, 8m^2\omega^2 - \ell(\ell+1); \xi) \\ & + C_2 \xi^{-2im\omega} e^{2im\omega\xi} HeunC(4im\omega, -4im\omega, 0, -8m^2\omega^2, 8m^2\omega^2 - \ell(\ell+1); \xi). \end{aligned} \tag{5.25}$$

This solution is then imposed to vanish at the mirror and at the positive infinity and the resulting equality is solved numerically for ω. The complex valued roots of this transcendental equation are the QNM frequencies. Thus, they can be compared to the results obtained by the simulation in order to validate the quality of the solution.

Looking at table 1 the agreement between the real frequency for both methods is reasonable, while the imaginary part has a higher disagreement with a maximum discrepancy at 1.4%. This proves a reasonable agreement between the two methods, leading to a confidence in the working of the simulation. This disagreement will be further on used as an estimate of the mean error for the magnetized cases.

A second sanity analysis possible in this limit is the verification of the power-law decay. While the quasi-normal modes depend heavily on the vicinity of the peak of potential, the major contribution of the power-law tail is due to the $1/r^2$ factor in the potential as discussed in the last chapter. As such, its behavior is not expected to largely deviate from that of a perturbation of a Schwarzschild black hole. Table 2 shows the measured power-law coefficients and how they compare to the expected value $\gamma = -6$.

Thus, in light of the good fit for the power-law tail as well as the real part of the frequency for the QNM modes and taking into account the caveats for the comparison between the methods of analysis, the results of the simulation can be considered solid.

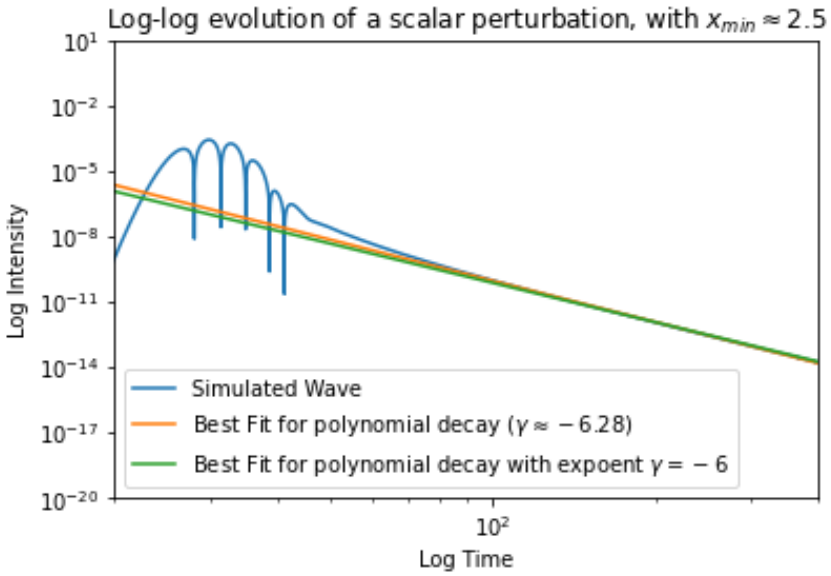

Figure 12 – Log-log graph of the time evolution of a QNM for the null magnetic field limit with the mirror at coordinate position $x = 2.5$ (or the tortoise coordinate equivalent $\tilde{x} \approx 0.114$). The orange line fits the power law coefficient, while the green line assumes the theoretical value and just fits an adequate initial amplitude.

5.4 Magnetized Stars

Once the sanity of the results from the simulation has been considered, the cases of interest can be analyzed, i.e., those containing a magnetized object. Each object can be characterized by two parameters, the radius of the sphere, i.e., the location of the mirror, and the α parameter related to the magnetic dipole moment by the equation (3.46b). By fixing $k = 1$, as done in chapter 3, this also implies that the mass will change as α changes according to equation (3.46a). Moreover, the choice of the radius of the star also limits how large the magnetic field can become, as the singularities will reach further from the horizon. Conversely, as discussed in the previous section, a larger radius means a smaller interaction between the wave and the potential peak leading to a shorter duration of the oscillating phase. As such, to observe the influence of the magnetic dipole in the QNM of this metric, an intermediary range of radii should be chosen.

The simulations were performed for three different positions of the mirror: -5, -10, and -15 in tortoise coordinates. The values of alpha were chosen in equal intervals until a value which made the solution almost singular. For $\tilde{x}_{min} = -5$ this meant $\alpha_{max} = 0.16$, while for $\tilde{x}_{min} = -10$ the value was $\alpha_{max} = 0.045$, and, finally, $\alpha_{max} = 0.012$ for $\tilde{x}_{min} = -15$. At last, the value of -5 was selected as the largest to be simulated, since the extraction of the QNMs become harder and less precise around this size of star for this metric.

All three cases presented decaying modes for all tested values of α. In fact, the stronger the magnetic dipole, the more negative the imaginary frequency of the QNM

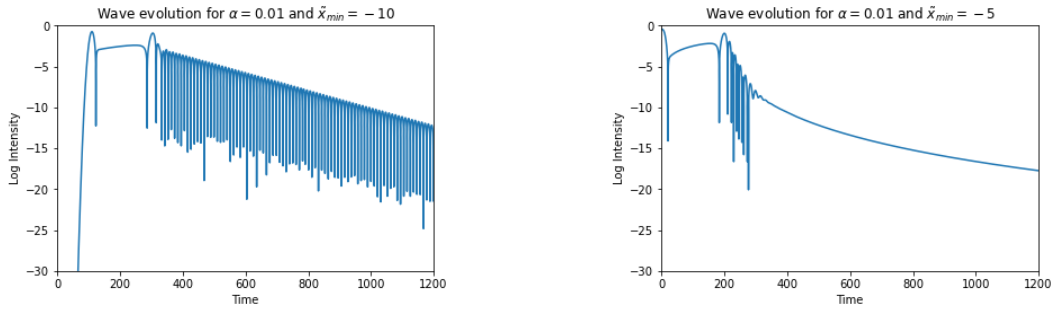

(a) $\tilde{x}_{min} = -10$ (b) $\tilde{x}_{min} = -05$

Figure 13 – Wave profile for the evolution of a scalar wave in a GM metric with $\alpha = 0.01$ and a mirror at positions -10 and -5 in tortoise coordinates.

became. As such the magnetic field has a stabilizing effect to this metric with respect to scalar perturbations. This confirms the expected results for an uncharged scalar field, as there is no first order time derivative term in the equation to account for the energy gain as usually required by superradiance.

The dependence on α of both the real and imaginary frequencies can be well approximated by a quadratic equation with a positive coefficient for the real part, while with a negative one for the imaginary part inside the observed range. This behavior would be expected, at least for small α, as both metric functions f and g depend explicitly only on the square of α. Yet, the behavior also holds for values of this parameter comparable to the limit of a regular star, $\alpha_{max} = \frac{1}{\sqrt{3}}$, as can be seen in image 16b. This, in turn, also means that they trace a line in the complex plane when α is varied inside this range, as can be seen in image 17.

The effect of the magnetic field, however, on the perturbations was small, on a scale of a hundredth to a few tenths of the frequency's value, and as such being much smaller than the effect of the size of star. Even in the maximum excursion of α studied in these runs, the real frequency differed by 5% from the non-magnetized case, while the imaginary frequency varied by about 15%. However, a variation of the mirror from $\tilde{x}_{min} = -10$ to $\tilde{x}_{min} = -5$, corresponding to a variation of 2% in the radius of the star, would produce a variation of a tenfold factor for the imaginary frequency and of about 30% for the real frequency.

Finally, the position of the mirror also influences the ring-down time of the oscillating behavior. As the surface of the star approaches the peak of the potential, the number of periods before the onset of the power-law tail reduces also for the magnetized case. In fact, the increase in the magnitude of the decaying factor with the magnetic field results in the oscillations dying out even faster. Conversely, the modes for smaller stars have longer ring-down times, as can be seen in figure 13. Thus, the results for $\tilde{x}_{min} = -5$ have few spatial points in which the wave could be analyzed.

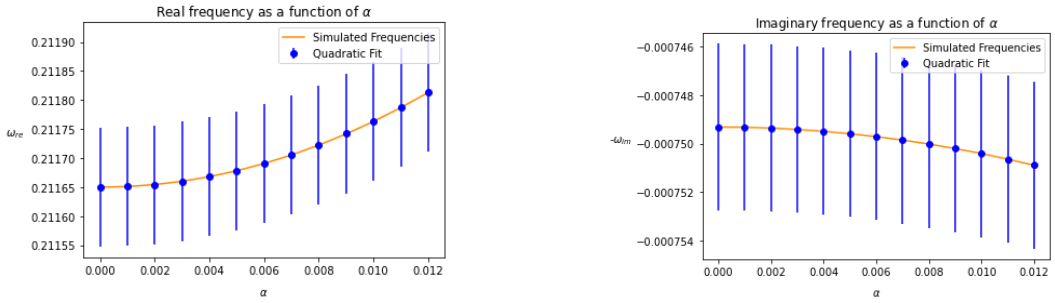

(a) Real Frequency (b) Imaginary Frequency

Figure 14 – Relation between the Magnetic Dipole parameter α and the real and imaginary frequencies for a star with radius $\tilde{x}_{min} = -15$ in tortoise coordinates. All dots have their respective error-bars, but for some it may be too small to be seen in the scale of the image.

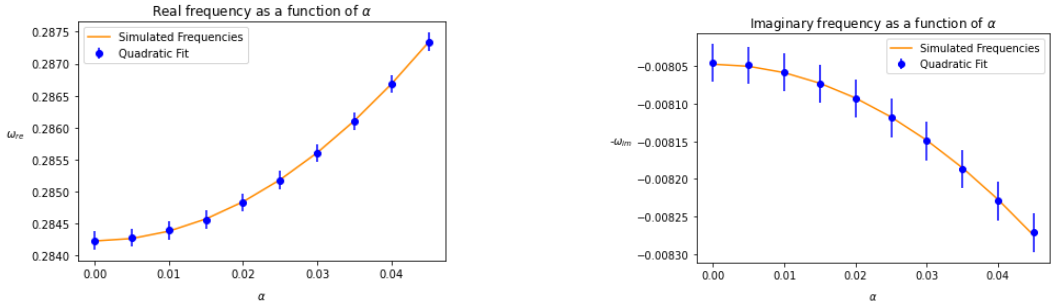

(a) Real Frequency (b) Imaginary Frequency

Figure 15 – Relation between the Magnetic Dipole parameter α and the real and imaginary frequencies for a star with radius $\tilde{x}_{min} = -10$ in tortoise coordinates. The fitted quadratic expression takes into account the estimated error-bars.

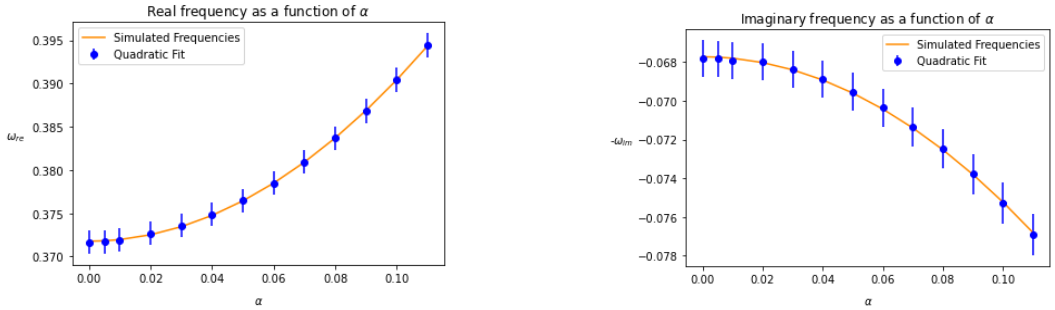

(a) Real Frequency (b) Imaginary Frequency

Figure 16 – Relation between the Magnetic Dipole parameter α and the real and imaginary frequencies for a star with radius $\tilde{x}_{min} = -5$ in tortoise coordinates.

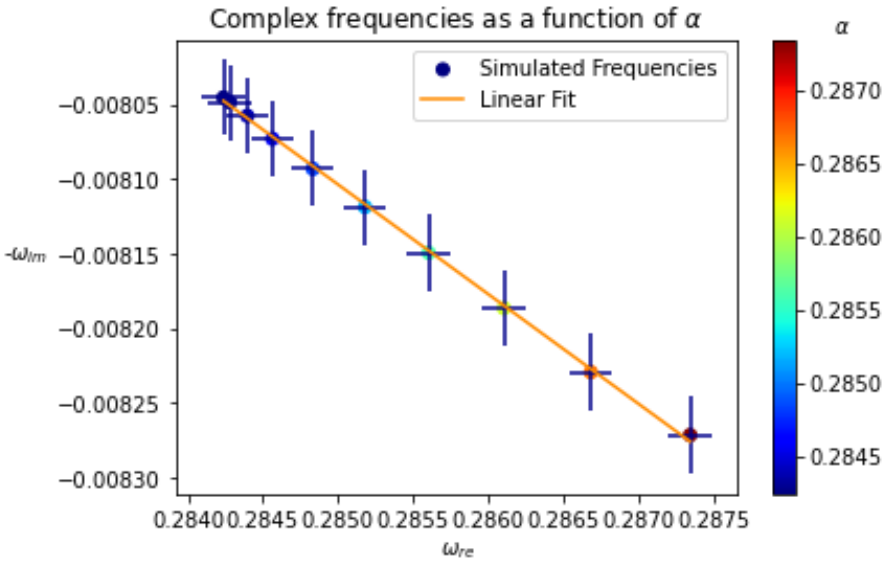

Figure 17 – The trace in the complex plane of the complex frequency as α is varied for a star with radius $\tilde{x}_{min} = -10$. Each point correspond to an observation with the line fitted to them in accordance to their error-bars.

6 Conclusions

This work has presented itself as an introduction to the perturbations of the Gutsunaev-Manko spacetime. The solution is derived from the Weyl Gauge and the requirement of an stationary axisymetric electrovacuum metric containing a magnetic dipole. Its internal structure has been studied. A brief review of perturbations in General Relativity is stated and subsequently particularized to the case of scalar matter fields. The equations of motion for these fields are developed and the partial wave equations were found in a suitable format. Finally, the numerical methods used for analysis are discussed and the obtained results are presented.

This solution was chosen for this study as a possible candidate for the mechanism of emission of FRB, in line with current hypothesis on its origin, due to its non-perturbative treatment of the magnetic field, a major aspect of many explanatory models for the explosive phenomenon. As such, a description of the radiative properties of the underlying objects can provide insights for the interpretation of the results expected from new generations of radio-telescopes, especially for BINGO.

The Gutsunaev-Manko metric, however, has naked singularities. These are just outside and touch The north pole of the horizon, which means that the plausibility as a black hole solution is low as the spacetime is not properly defined there. They can, however, be viable descriptions of the exterior field of some Neutron Stars, in particular, those with low angular momentum.

This solution forms a natural extension of the Schwarzschild Metric and can be related back to it by the introduction of two new functions into the line element under suitable prolate coordinates. The regular black hole is, in fact, the limit for a null magnetic field. As such, the Geodesics remain similar, specially on the equatorial plane. However, outside this plane there are no purely radial null geodesics, which instead curve towards the equator as it approaches the horizon. That deviation is still not very large.

As for its perturbations, the metric ones are coupled to the electromagnetic ones. This means that electromagnetic waves induce gravitational waves or vice versa, which require solving both perturbative equations simultaneously. Yet, the separation of axial and polar perturbations is still possible, due to the reflection symmetry at the equator. However, the different angular momenta are intrinsically mixed. For a scalar field these problems were still present, but were more tractable due to the existence of a single free variable. In this case the addition of charge caused a small effect and in both uncharged and charged scenarios the dynamics was determined by gravity.

The coupled modes were not suited for the WKB method, thus, rather the Finite

Differences were used. The interior of the star was not considered, instead opting for a perfectly reflective surface called a mirror along this work. This reduced the complexity of adding an internal solution. We worked with the tortoise coordinates at the expense of a less physical model.

As for consistency of the numerical solution, the results were compared in the limiting case of a Schwarzschild metric with a perfectly reflecting Black Hole. This showed a good agreement of both the real and imaginary parts of the frequency. The relative error could then be used as an estimation of the uncertainty to the measured values for the frequency in the magnetized case.

With these results in mind, the magnetized cases were simulated. The parameters were varied for both the radius of the surface of the star as well as the magnetic field. The analysis of this object's QNMs demonstrated that for scalar fields no instability is present. This was expected, though, as the potential is always positive and there are no first-order time derivatives for the wave equation. Moreover, the effect of the magnetic field is much smaller than the effect due to the relative size of the star.

In contrast to some perturbatively unstable solutions of the Einstein-Maxwell equations, such as the RN-AdS black hole (Abdalla et al., 2019a), the addition of a charge had a small effect on the wave equations for the scalar field. There was a negative term in the potential, which, however, was much smaller than the gravitational contribution, and not enough to cause a negative well to the full potential.

Finally, the relation of the magnetic dipole through the α parameter with both real and imaginary parts of the quasinormal frequencies could be approximated by a quadratic curve inside the range of values that were studied. This also means that they trace straight lines across the complex plane as α is varied for each fixed position for the surface of the star.

Therefore, the perturbations of scalar fields on a Gutsunaev-Manko background do not suffice for a description of FRBs, as they provide no explosive mechanism. However, they also represent the simplest case of perturbations involving the GM metric. This means that other types of perturbation could still be viable candidates. In particular, Spin-1/2, i.e., fermionic matter fields have a different coupling to gravity in terms of the spin connection. These can lead to equations of motion with the desired first-order time derivatives and is the next simplest case. Moreover, further solutions have been generated since GM's discovery, that extend the studied metric by including angular momentum and a mass quadrupole momentum. These further add mechanisms to the search of unstable perturbative modes.

As for the asteroseismology potential of studying QNMs of magnetized stars, an improvement in the certainty of the results would be beneficial. For the scalar perturbation

this can first be done by simulating a wider range of initial conditions and other variations for the parameters, such as keeping the mass constant instead of the scale factor of the prolate spheroidal coordinates. Moreover, the gravitational and electromagnetic perturbations should also be studied, as they represent the direct types of observation for these objects. Finally, more realistic interior solutions would represent a great improvement to this study providing a more appropriate boundary condition.

References

Abdalla, E. et al. Instability of a Reissner-Nordström-AdS black hole under perturbations of a scalar field coupled to the Einstein tensor. *Physical Review D*, American Physical Society, v. 99, n. 10, p. 104065, 2019. ISSN 24700029. Available on: <https://doi.org/10.1103/PhysRevD.99.104065>.

Abdalla, E.; Cuadros-Melgar, B.; Oliveira, J. D.; Pavan, A. B.; Pellicer, C. E. Vectorial and spinorial perturbations in Galileon black holes: Quasinormal modes, quasiresonant modes, and stability. *Physical Review D*, v. 99, n. 4, p. 1–25, 2019. ISSN 24700029.

Abdalla, E. et al. The BINGO project: I. Baryon acoustic oscillations from integrated neutral gas observations. *Astronomy and Astrophysics*, v. 664, p. 1–23, 2022. ISSN 14320746.

Adams, R. C.; Cary, B. B.; Cohen, J. M. A simple model of a supernova. *Astrophysics and Space Science*, v. 155, n. 2, p. 271–293, 1989. ISSN 0004-640X. Available on: <http://link.springer.com/10.1007/BF00643864>.

Aggarwal, K. et al. Comprehensive Analysis of a Dense Sample of FRB 121102 Bursts. *The Astrophysical Journal*, v. 922, n. 2, p. 115, 2021. ISSN 0004-637X.

Amiri, M. et al. The First CHIME/FRB Fast Radio Burst Catalog. *The Astrophysical Journal Supplement Series*, v. 257, n. 2, p. 59, 2021. ISSN 0067-0049.

Andersson, N. Evolving test fields in a black-hole geometry. *Physical Review D - Particles, Fields, Gravitation and Cosmology*, v. 55, n. 2, p. 468–479, 1997. ISSN 15502368.

Andersson, N.; Kokkotas, K. D. Towards gravitational wave asteroseismology. *Monthly Notices of the Royal Astronomical Society*, v. 299, n. 4, p. 1059–1068, 1998. ISSN 00358711.

Avez, A. Le ds2 de Schwarzschild parmi les ds2 stationnaires. *Annales de L'Institut Henri Poincare-physic theorique*, v. 1, p. 291–300, 1964.

Baryakhtar, M.; Galanis, M.; Lasenby, R.; Simon, O. Black hole superradiance of self-interacting scalar fields. *Physical Review D*, v. 103, n. 9, 2021. ISSN 24700029.

Baumgarten, T. W.; Shapiro, S. L. *Numerical Relativity: Solving Einstein's Equations on the ComputerNumerical Relativity: Solving Einstein's Equations on the Computer*. : Cambridge University Press, 2010. 698 p. ISBN 978-0-521-51407-1.

Bekenstein, J. D. Black Holes: Classical Properties, Thermodynamics and Heuristic Quantization. 1998. Available on: <http://arxiv.org/abs/gr-qc/9808028>.

Benone, C. L.; Crispino, L. C. Superradiance in static black hole spacetimes. *Physical Review D*, v. 93, n. 2, p. 1–6, 2016. ISSN 24700029.

Bethapudi, S.; Spitler, L. G.; Main, R. A.; Li, D. Z.; Wharton, R. S. High frequency study of FRB 20180916B using the 100-m Effelsberg radio telescope. *Monthly Notices of the Royal Astronomical Society*, v. 524, n. 3, p. 3303–3313, 2023. ISSN 13652966.

Brito, R.; Cardoso, V.; Pani, P. *Superradiance*. Cham: Springer International Publishing, 2020. v. 971. (Lecture Notes in Physics, v. 971). ISBN 978-3-030-46621-3. Available on: <http://arxiv.org/abs/1501.06570%0Ahttp://dx.doi.org/10.1007/978-3-030-46622-0http://link.springer.com/10.1007/978-3-030-46622-0>.

Chandrasekhar, S. The Mathematical Theory of Black Holes. In: *General Relativity and Gravitation*. Dordrecht: Springer Netherlands, 1984. v. 306, n. 3, p. 5–26. ISBN 978-0198503705. Available on: <https://onlinelibrary.wiley.com/doi/10.1002/asna.2113060308http://link.springer.com/10.1007/978-94-009-6469-3_2>.

Chen, S.; Jing, J. Dynamical evolution of a scalar field coupling to Einstein's tensor in the Reissner-Nordström black hole spacetime. *Physical Review D - Particles, Fields, Gravitation and Cosmology*, v. 82, n. 8, p. 1–7, 2010. ISSN 15507998.

Ching, E. S.; Leung, P. T.; Suen, W. M.; Young, K. Wave propagation in gravitational systems: Completeness of quasinormal modes. *Physical Review D - Particles, Fields, Gravitation and Cosmology*, v. 54, n. 6, p. 3778–3791, 1996. ISSN 15502368.

Ching, E. S. C.; Leung, P. T.; Suen, W. M.; Young, K. Wave propagation in gravitational systems: Late time behavior. *Physical Review D*, v. 52, n. 4, p. 2118–2132, 8 1995. ISSN 0556-2821. Available on: <https://link.aps.org/doi/10.1103/PhysRevD.52.2118>.

Colgate, S. A.; White, R. H. The Hydrodynamic Behavior of Supernovae Explosions. *The Astrophysical Journal*, v. 143, n. population II, p. 626, 3 1966. ISSN 0004-637X. Available on: <http://adsabs.harvard.edu/doi/10.1086/148549>.

Cordes, J. M.; Chatterjee, S. Fast Radio Bursts: An Extragalactic Enigma. *Annual Review of Astronomy and Astrophysics*, v. 57, p. 417–465, 2019. ISSN 00664146.

Delgaty, M. S.; Lake, K. Physical acceptability of isolated, static, spherically symmetric, perfect fluid solutions of Einstein's equations. *Computer Physics Communications*, v. 115, n. 2-3, p. 395–415, 1998. ISSN 00104655.

Dodelson, S.; Schmidt, F. *Modern Cosmology, Second Edition*. 2020. 1–494 p. ISBN 9780128159484.

Ernst, F. J. New Formulation of the Axially Symmetric Gravitational Field Problem. *Physical Review*, v. 167, n. 5, p. 1175–1178, 3 1968. ISSN 0031-899X. Available on: <https://link.aps.org/doi/10.1103/PhysRev.167.1175>.

Ernst, F. J. New formulation of the axially symmetric gravitational field problem. II. *Physical Review*, v. 168, n. 5, p. 1415–1417, 1968. ISSN 0031899X.

Ferrari, V.; Mashhoon, B. New approach to the quasinormal modes of a black hole. *Physical Review D*, v. 30, n. 2, p. 295–304, 1984. ISSN 05562821.

Ferrari, V.; Mashhoon, B. Oscillations of a black hole. *Physical Review Letters*, v. 52, n. 16, p. 1361–1364, 1984. ISSN 00319007.

Filho, E. d. C. *Construction of new solutions of the electro-vacuum Einstein equation*. Tese (Doutorado) — Universidade de São Paulo, 2020.

Fiziev, P. P. Exact Solutions of Regge-Wheeler Equation and Quasi-Normal Modes of Compact Objects. 9 2005. Available on: <http://arxiv.org/abs/gr-qc/0509123http://dx.doi.org/10.1088/0264-9381/23/7/015>.

Freitas, V. P. D. Discos Relativ´ ısticos Auto-Gravitantes: Aspectos de Estabilidade. 2013.

Gajjar, V. et al. Highest Frequency Detection of FRB 121102 at 4–8 GHz Using the Breakthrough Listen Digital Backend at the Green Bank Telescope. *The Astrophysical Journal*, IOP Publishing, v. 863, n. 1, p. 2, 2018. ISSN 15384357. Available on: <http://dx.doi.org/10.3847/1538-4357/aad005>.

Gal'tsov, D. V.; Matiukhin, A. A. Matrix WKB method for black hole normal modes and quasibound states. *Classical and Quantum Gravity*, v. 9, n. 9, p. 2039–2055, 9 1992. ISSN 0264-9381. Available on: <https://iopscience.iop.org/article/10.1088/0264-9381/9/9/009>.

Greene, B. R.; Mathur, S. D.; O'Neill, C. M. Eluding the no-hair conjecture: Black holes in spontaneously broken gauge theories. *Physical Review D*, v. 47, n. 6, p. 2242–2259, 1993. ISSN 05562821.

Greene, B. R.; Mathur, S. D.; O'Neill, C. M. Eluding the no-hair conjecture: Black holes in spontaneously broken gauge theories. *Physical Review D*, v. 47, n. 6, p. 2242–2259, 1993. ISSN 05562821.

Griffiths, J. B.; Podolský, J. *Exact Space-Times in Einstein's General Relativity*. Cambridge University Press, 2009. ISBN 9780521889278. Available on: <https://www.cambridge.org/core/product/identifier/9780511635397/type/book>.

Gundlach, C.; Price, R. H.; Pullin, J. Late-time behavior of stellar collapse and explosions. II. Nonlinear evolution. *Physical Review D*, v. 49, n. 2, p. 890–899, 1994. ISSN 05562821.

Gutsunaev, T. I.; Manko, V. S. On the gravitational field of a mass possessing a magnetic dipole moment. *Physics Letters A*, v. 123, n. 5, p. 215–216, 1987. ISSN 03759601.

Gutsunaev, T. I.; Manko, V. S. On a family of solutions of the Einstein-Maxwell equations. *General Relativity and Gravitation*, v. 20, n. 4, p. 327–335, 1988. ISSN 00017701.

Hessels, J. W. T. et al. FRB 121102 Bursts Show Complex Time–Frequency Structure. *The Astrophysical Journal*, v. 876, n. 2, p. L23, 2019. ISSN 20418213.

Heusler, M. Stationary Black Holes: Uniqueness and Beyond Living Reviews in Relativity Article Amendments. 1998. Available on: <http://www-theorie.physik.unizh.ch/Ëœheusler/www.livingreviews.org/Articles/Volume1/1998-6heuslerhttp://www.livingreviews.org/Articles/Volume1/1998-6heusler/.>

Jeffery, G. B. The field of an electron on Einstein's theory of gravitation. *Proceedings of the Royal Society of London. Series A, Containing Papers of a Mathematical and Physical Character*, v. 99, n. 697, p. 123–134, 5 1921. ISSN 0950-1207. Available on: <https://royalsocietypublishing.org/doi/10.1098/rspa.1921.0028>.

Kerr, R. P. Gravitational field of a spinning mass as an example of algebraically special metrics. *Physical Review Letters*, v. 11, n. 5, p. 237–238, 1963. ISSN 00319007.

Kirsten, F. et al. Connecting repeating and non-repeating fast radio bursts via their energy distributions. 2023. Available on: <http://arxiv.org/abs/2306.15505>.

Kleihaus, B.; Kunz, J. Static black-hole solutions with axial symmetry. *Physical Review Letters*, v. 79, n. 9, p. 1595–1598, 1997. ISSN 10797114.

Kokkotas, K. D. Quasi-Normal Modes of Stars and Black Holes. 1999.

Kolyvaris, T.; Koukouvaou, M.; Machattou, A.; Papantonopoulos, E. Superradiant instabilities in scalar-tensor Horndeski theory. *Physical Review D*, v. 98, n. 2, p. 1–21, 2018. ISSN 24700029.

Kolyvaris, T.; Koutsoumbas, G.; Papantonopoulos, E.; Siopsis, G. A new class of exact hairy black hole solutions. *General Relativity and Gravitation*, v. 43, n. 1, p. 163–180, 2011. ISSN 15729532.

Kolyvaris, T.; Papantonopoulos, E. Superradiant Amplification of a Scalar Wave Coupled Kinematically to Curvature Scattered off a Reissner-Nordstr\"om Black Hole. p. 1–12, 2017. Available on: <http://arxiv.org/abs/1702.04618>.

Konoplya, R. A.; Stuchlík, Z.; Zhidenko, A. Massive nonminimally coupled scalar field in Reissner-Nordström spacetime: Long-lived quasinormal modes and instability. *Physical Review D*, v. 98, n. 10, p. 1–8, 2018. ISSN 24700029.

Konoplya, R. A.; Zhidenko, A. Quasinormal modes of black holes: From astrophysics to string theory. *Reviews of Modern Physics*, v. 83, n. 3, p. 793–836, 2011. ISSN 00346861.

Konoplya, R. A.; Zhidenko, A. Charged scalar field instability between the event and cosmological horizons. *Physical Review D - Particles, Fields, Gravitation and Cosmology*, v. 90, n. 6, p. 1–6, 2014. ISSN 15502368.

Konoplya, R. A.; Zhidenko, A. First few overtones probe the event horizon geometry. p. 1–6, 9 2022. Available on: <http://arxiv.org/abs/2209.00679>.

Konoplya, R. A.; Zhidenko, A.; Zinhailo, A. F. Higher order WKB formula for quasinormal modes and grey-body factors: Recipes for quick and accurate calculations. *Classical and Quantum Gravity*, v. 36, n. 15, p. 1–15, 2019. ISSN 13616382.

Koutsoumbas, G.; Mitsoulas, I.; Papantonopoulos, E. Quantum effects in Galileon black holes. *Classical and Quantum Gravity*, v. 35, n. 23, p. 1–11, 2018. ISSN 13616382.

Künzle, H. P. On the spherical symmetry of a static perfect fluid. *Communications in Mathematical Physics*, v. 20, n. 2, p. 85–100, 1971. ISSN 00103616.

Laarakkers, W. G.; Poisson, E. Quadrupole moments of rotating neutron stars. p. 1–7, 1998.

Lavrelashvili, G.; Maison, D. of Einstein — Yang — Mills dilaton theory Regular and. v. 410, 1993.

Leaver, E. W. Spectral decomposition of the perturbation response of the Schwarzschild geometry. *Physical Review D*, v. 34, n. 2, p. 384–408, 1986. ISSN 05562821.

Levander, A. R. Fourth-order finite-difference P-SV seismograms. *Geophysics*, v. 53, n. 11, p. 1425–1436, 1988. ISSN 00168033.

Li, D. et al. A bimodal burst energy distribution of a repeating fast radio burst source. *Nature*, v. 598, n. 7880, p. 267–271, 10 2021. ISSN 0028-0836. Available on: <https://www.nature.com/articles/s41586-021-03878-5>.

Lorimer, D. R.; Bailes, M.; McLaughlin, M. A.; Narkevic, D. J.; Crawford, F. A bright millisecond radio burst of extragalactic origin. *Science*, v. 318, n. 5851, p. 777–780, 2007. ISSN 00368075.

Maggiore, M. *A Modern introduction to quantum field theory*. 2005. ISBN 9780198520740.

Maggiore, M. *Michele Maggiore: Gravitational waves. Volume 1: theory and experiments*. 2008. v. 1. ISBN 978-0-19-857074-5.

Maggiore, M. *Gravitational waves: Volume 2: Astrophysics and cosmology*. 2018. 1–820 p. ISBN 9780198570899.

Manko, V. S. On a general static axisymmetric solution of the Einstein vacuum equations. *General Relativity and Gravitation*, v. 21, n. 11, p. 1193–1195, 1989. ISSN 00017701.

Manko, V. S. New generalization of the Kerr metric referring to a magnetized spinning mass. *Classical and Quantum Gravity*, v. 10, n. 12, 1993. ISSN 02649381.

Manko, V. S.; Mielke, E. W.; Sanabria-Gómez, J. D. Exact solution for the exterior field of a rotating neutron star. *Physical Review D - Particles, Fields, Gravitation and Cosmology*, v. 61, n. 8, p. 1–5, 2000. ISSN 15502368.

Manko, V. S.; Sibgatullin, N. R. Exact solution of the Einstein-Maxwell equations for the exterior gravitational field of a magnetized rotating mass. *Physical Review D*, v. 46, n. 10, p. 4122–4124, 1992. ISSN 05562821.

Manko, V. S.; Sibgatullin, N. R. Metric of a rotating, charged, magnetised mass. *Physics Letters A*, v. 168, n. 5-6, p. 343–347, 1992. ISSN 03759601.

Matyjasek, J.; Opala, M. Quasinormal modes of black holes: The improved semianalytic approach. *Physical Review D*, v. 96, n. 2, p. 20–31, 2017. ISSN 24700029.

Matyjasek, J.; Telecka, M. Quasinormal modes of black holes. II. Padé summation of the higher-order WKB terms. *Physical Review D*, v. 100, n. 12, p. 1–11, 2019. ISSN 24700029.

Menza, L. D.; Nicolas, J. P. Superradiance on the Reissner-Nordstrøm metric. *Classical and Quantum Gravity*, v. 32, n. 14, p. 1–31, 2015. ISSN 13616382.

Metzger, B. D.; Berger, E.; Margalit, B. Millisecond Magnetar Birth Connects FRB 121102 to Superluminous Supernovae and Long-duration Gamma-Ray Bursts. *The Astrophysical Journal*, v. 841, n. 1, p. 14, 2017. ISSN 15384357.

Miller, J. M.; Miller, M. C.; Reynolds, C. S. The angular momenta of neutron stars and black holes as a window on supernovae. *Astrophysical Journal Letters*, v. 731, n. 1 PART II, p. 1–5, 2011. ISSN 20418213.

Minamitsuji, M. Black hole quasinormal modes in a scalar-tensor theory with field derivative coupling to the Einstein tensor. *General Relativity and Gravitation*, v. 46, n. 9, p. 1–10, 2014. ISSN 15729532.

Misner, C. W.; Thorne, K. S.; Wheeler, J. A. *Gravitation*. San Francisco: W. H. Freeman, 1973. ISBN 9780691177793.

Molina, C.; Giugno, D.; Abdalla, E.; Saa, A. Field propagation in de Sitter black holes. *Physical Review D - Particles, Fields, Gravitation and Cosmology*, v. 69, n. 10, 2004. ISSN 15502368.

Newman, E. T. et al. Metric of a rotating, charged mass. *Journal of Mathematical Physics*, v. 6, n. 6, p. 918–919, 1965. ISSN 00222488.

Newman, E. T.; Janis, A. I. Note on the Kerr spinning-particle metric. *Journal of Mathematical Physics*, v. 6, n. 6, p. 915–917, 1965. ISSN 00222488.

Nollert, H. P. Quasinormal modes: The characteristic 'sound' of black holes and neutron stars. *Classical and Quantum Gravity*, v. 16, n. 12, 1999. ISSN 02649381.

Nordström, G. On the Energy of the Gravitation field in Einstein's Theory. *Proceeding of Royal Netherlands Academy of Arts and Sciences (KNAW)*, 1918.

Oppenheimer, J. R.; Volkoff, G. M. On massive neutron cores. *Physical Review*, v. 55, n. 4, p. 374–381, 1939. ISSN 0031899X.

Penrose, R.; Floyd, R. M. Extraction of Rotational Energy from a Black Hole. *Nature Physical Science*, v. 229, n. 6, p. 177–179, 1971. ISSN 0300-8746.

Petroff, E. et al. FRBCAT: The fast radio burst catalogue. *Publications of the Astronomical Society of Australia*, v. 33, p. 1–7, 2016. ISSN 14486083.

Platts, E. et al. A living theory catalogue for fast radio bursts. *Physics Reports*, v. 821, p. 1–27, 2019. ISSN 03701573.

Poisson, E. *A Relativist's Toolkit: The Mathematics of Black-Hole Mechanics*. Cambridge University Press, 2004. ISBN 9780511606601. Available on: <https://www.cambridge.org/core/product/identifier/9780511606601/type/book>.

Pound, A.; Wardell, B. Black Hole Perturbation Theory and Gravitational Self-Force. *Handbook of Gravitational Wave Astronomy*, p. 1–119, 2021.

Price, R. H. Nonspherical perturbations of relativistic gravitational collapse. II. Integer-spin, zero-rest-mass fields. *Physical Review D*, v. 5, n. 10, p. 2439–2454, 1972. ISSN 05562821.

Price, R. H.; Pullin, J. Colliding black holes: The close limit. *Physical Review Letters*, v. 72, n. 21, p. 3297–3300, 1994. ISSN 00319007.

Regge, T.; Wheeler, J. A. Stability of a schwarzschild singularity. *Physical Review*, v. 108, n. 4, p. 1063–1069, 1957. ISSN 0031899X.

Reissner, H. Über die Eigengravitation des elektrischen Feldes nach der Einsteinschen Theorie. *Annalen der Physik*, v. 355, n. 9, p. 106–120, 1 1916. ISSN 0003-3804. Available on: <https://onlinelibrary.wiley.com/doi/10.1002/andp.19163550905>.

Ribeiro, E. M. C. D. *Perturbações escalares em espaços-tempos axialmente simétricos*. Tese (Doutorado) — Universidade de São Paulo, 2024.

Ridgway, S. A.; Weinberg, E. J. Static black hole solutions without rotational symmetry. *Physical Review D*, v. 52, n. 6, p. 3440–3456, 1995. ISSN 05562821.

Rybicki, G. B.; Lightman, A. P. *Radiaitve Processes In Astrophysics*. 1979. ISBN 9780471827597. Available on: <https://ui.adsabs.harvard.edu/abs/1979rpa..book.....R/abstract>.

Ryutov, D. D. Using plasma physics to weigh the photon. *Plasma Physics and Controlled Fusion*, v. 49, n. 12 B, 2007. ISSN 07413335.

Sakurai, J. J.; Napolitano, J. *Sakuraii-Modern Quantum Mechanics*. 2012. 550 p. ISBN 9780805382914.

Schutz, B. F.; Will, C. M. Black hole normal modes - A semianalytic approach. *The Astrophysical Journal*, v. 291, n. c, p. L33, 1985. ISSN 0004-637X.

Schwarzschild, K. On the gravitational field of a sphere of incompressible fluid according to Einstein's theory. 12 1999. Available on: <http://arxiv.org/abs/physics/9912033>.

Schwarzschild, K. On the Gravitational Field of a Mass Point according to Einstein's Theory. *General Relativity and Gravitation*, v. 35, n. 5, p. 951–959, 5 2003. ISSN 00017701. Available on: <http://arxiv.org/abs/physics/9905030>.

Starobinskiĭ, A. Amplification of waves during reflection from a rotating "black hole

. *Soviet Journal of Experimental and Theoretical Physics*, v. 37, n. 1, p. 28 – 32, 1973. ISSN 1063-7761.

Stephani, H.; Kramer, D.; MacCallum, M.; Hoenselaers, C.; Herlt, E. *Exact Solutions of Einstein's Field Equations*. Cambridge University Press, 2003. v. 16. 958–960 p. ISSN 00222488. ISBN 9780521461368. Available on: <https://www.cambridge.org/core/product/identifier/9780511535185/type/book>.

Taub, A. H. Space-times with distribution valued curvature tensors. *Journal of Mathematical Physics*, v. 21, n. 6, p. 1423–1431, 1979. ISSN 00222488.

Teukolsky, S. A.; Press, W. H. Perturbations of a rotating black hole III. *Astrophysical Journal*, v. 193, n. 1967, p. 443–461, 1974.

Tolman, R. C. Static Solutions of Einstein's Field Equations for Spheres of Fluid. *Physical Review*, v. 55, n. 4, p. 364–373, 2 1939. ISSN 0031-899X. Available on: <https://link.aps.org/doi/10.1103/PhysRev.55.364>.

Vaidya, P. C. The gravitational field of a radiating star. *Proceedings of the Indian Academy of Sciences - Section A*, v. 33, n. 5, p. 264–276, 1951. ISSN 03700089.

Vishveshwara, C. V. Scattering of Gravitational Radiation by a Schwarzschild Black-hole. *Nature*, v. 227, n. 5261, p. 936–938, 8 1970. ISSN 0028-0836. Available on: <https://www.nature.com/articles/227936a0>.

Wald, R. M. *General Relativity*. University of Chicago Press, 1984. ISBN 9780226870335. Available on: <http://www.bibliovault.org/BV.landing.epl?ISBN=9780226870335>.

Wald, R. M. *Quantum field theory in curved spacetime and black hole thermodynamics*. : University of Chicago Press, 1995. ISBN 0-226-87027-8.

Weinberg, S. *Cosmology*. 2008. 593 p. ISBN 9780198526827.

Weyl, H. Zur Gravitationstheorie. *Annalen der Physik*, v. 359, n. 18, p. 117–145, 1917. ISSN 15213889.

Yu, S.; Gao, C. Quasinormal modes of static and spherically symmetric black holes with the derivative coupling. *General Relativity and Gravitation*, v. 51, n. 1, 2019. ISSN 15729532.

Zel'dovich, Y. B. Generation of Waves by a Rotating Body. *Soviet Journal of Experimental and Theoretical Physics Letters*, v. 14, p. 180, 1971. Available on: <http://adsabs.harvard.edu/cgi-bin/nph-data_query?bibcode=1971ZhPmR..14..270Z&link_type=EJOURNAL%0Apapers3://publication/uuid/683B33C7-7F82-4AD4-8AF0-8B2F289E1BD4>.

Zel'dovich, Y. B.; Novikov, I. D.; Silk, J. Relativistic Astrophysics, Vol. 1: Stars and Relativity. *Physics Today*, v. 25, n. 3, p. 63–64, 3 1972. ISSN 0031-9228. Available on: <https://pubs.aip.org/physicstoday/article/25/3/63/428441/Relativistic-Astrophysics-Vol-1-Stars-and>.

Zerilli, F. J. Gravitational field of a particle falling in a schwarzschild geometry analyzed in tensor harmonics. *Physical Review D*, v. 2, n. 10, p. 2141–2160, 1970. ISSN 05562821.

Zhang, B. The physical mechanisms of fast radio bursts. *Nature*, v. 587, n. 7832, p. 45–53, 11 2020. ISSN 0028-0836. Available on: <http://www.nature.com/articles/s41586-020-2828-1>.

Zhu, Z.; Zhang, S. J.; Pellicer, C. E.; Wang, B.; Abdalla, E. Stability of Reissner-Nordström black hole in de Sitter background under charged scalar perturbation. *Physical Review D - Particles, Fields, Gravitation and Cosmology*, v. 90, n. 4, p. 1–15, 2014. ISSN 15502368.

APPENDIX A – Connection and Curvature for Gutsanaev-Manko Metric

The geometry of the Gutsunaev-Manko solution can be seen in the Mathematica script linked at:

<https://github.com/LucasFormigari/Gutsunaev-Manko-Curvature-Mathematica>

The python codes used to simulate the evolution of the wave can be found in the repository:

<https://github.com/LucasFormigari/finite_elements_gm>

A.1 Christoffel Symbol

A.1.1 Implicit

$$\Gamma^0_{10} = \frac{1}{x^2-1} + \frac{\partial_x f}{f}$$

$$\Gamma^0_{20} = \frac{\partial_y f}{f}$$

$$\Gamma^1_{00} = \frac{(x-1)f^3\left(f+(x^2-1)\partial_x f\right)}{(x+1)^3 g^2}$$

$$\Gamma^1_{11} = -\frac{1}{x^2-1} - \frac{\partial_x f}{f} + \frac{\partial_x g}{g}$$

$$\Gamma^1_{12} = -\frac{\partial_y f}{f} + \frac{\partial_y g}{g}$$

$$\Gamma^1_{22} = +\frac{(x^2-1)\partial_x f}{f} - \frac{x-1}{1-y^2} - \frac{(x^2-1)\partial_x f}{(1-y^2)g}$$

$$\Gamma^1_{33} = -16\frac{(x-1)(1-y^2)(f-(x+1)\partial_x f)}{g^2}$$

$$\Gamma^2_{00} = \frac{(x-1)(1-y^2)f^3\partial_y f}{(x+1)^3 g^2}$$

$$\Gamma^2_{11} = \frac{(1-y^2)}{(x^2-1)}\left[\frac{\partial_y f}{f} - \frac{\partial_y g}{g}\right]$$

$$\Gamma^2_{12} = \frac{1}{x+1} - \frac{\partial_x f}{f} + \frac{\partial_x g}{g}$$

$$\Gamma^2_{22} = \frac{y}{1-y^2} - \frac{\partial_y f}{f} + \frac{\partial_y g}{g}$$

$$\Gamma^2_{33} = 16\frac{(1-y^2)\big(f-(1-y^2)\partial_y f\big)}{fg^2}$$

$$\Gamma^3_{13} = \frac{1}{x+1} - \frac{\partial_x f}{f}$$

$$\Gamma^3_{23} = -\frac{y}{1-y^2} - \frac{\partial_y f}{f}$$

A.2 Ricci Curvature Tensor

A.2.1 Implicit

$$\mathrm{R}_{00} = -\frac{(x-1)f^2\big\{(1-y^2)(\partial_y f)^2+(x^2-1)(\partial_x f)^2+f\big[2y\partial_y f-(1-y^2)\partial_y^2 f-2x\partial_x f-(x^2-1)\partial_x^2 f\big]\big\}}{(x+1)^3 g^2}$$

$$R_{11} = -\frac{(1-y^2)(\partial_y f)^2+3(x^2-1)(\partial_x f)^2}{(x^2-1)f^2} + \frac{-2y\partial_y f+(1-y^2)\partial_y^2 f-4\partial_x f+2x\partial_x f-\partial_x^2 f+x^2\partial_x^2}{(x^2-1)f}$$

$$+ \frac{(1-y^2)(\partial_y g)^2+(x^2-1)(\partial_x g)^2+g(2y\partial_y g-(1-y^2)\partial_y^2 g-(x^2-1)\partial_x^2 g)}{(x^2-1)g^2}$$

$$R_{12} = -\frac{2(1-y^2)fg\partial_y f-2(x^2-1)(1-y^2)g(\partial_x f)(\partial_y f)+f^2(-x(1-y^2)\partial_y g+(x^2-1)y\partial_x g)}{(x^2-1)(1-y^2)f^2 g}$$

$$R_{22} = -\frac{3(1-y^2)(\partial_y f)^2+(x^2-1)(\partial_x f)^2}{(1-y^2)f^2} - \frac{2y\partial_y f-(1-y^2)\partial_y^2 f-2x\partial_x f-(x^2-1)\partial_x^2 f}{(1-y^2)f}$$

$$+ \frac{(1-y^2)(\partial_y g)^2+(x^2-1)(\partial_x g)^2}{(1-y^2)g^2} - \frac{(1-y^2)\partial_y^2 g+2x\partial_x g+(x^2-1)\partial_x^2 g}{(1-y^2)g}$$

$$R_{33} = -16\frac{(1-y^2)}{f^2 g^2}\left\{(1-y^2)(\partial_y f)^2 + (x^2-1)(\partial_x f)^2 + f\left[2y\partial_y f - (1-y^2)\partial_y^2 f - 2x\partial_x f - (x^2-1)\partial_x^2 f\right]\right\}$$